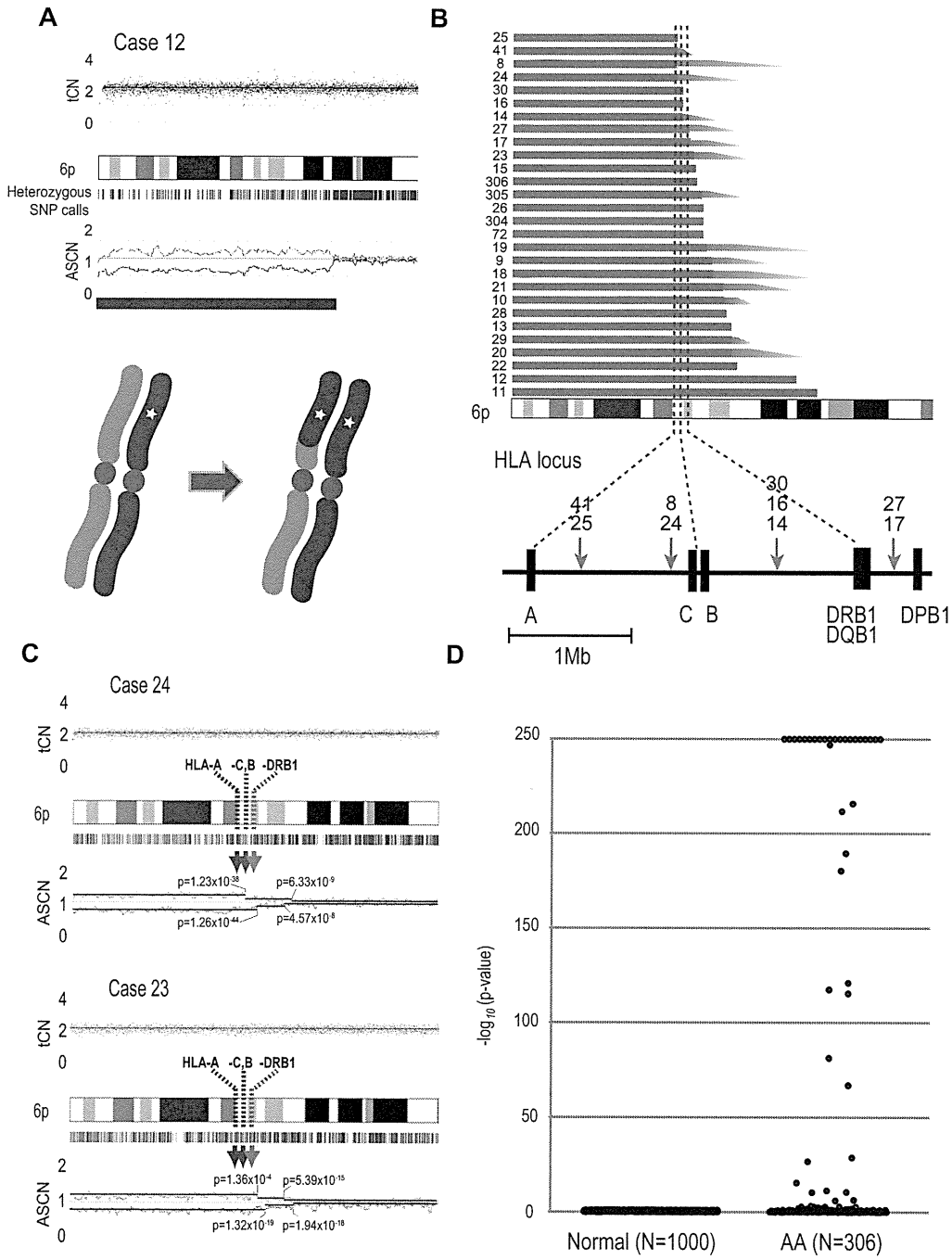

Figure 2. Acquired 6pLOHs in AA patients that target the HLA locus. (A) Typical CNAG outputs in SNP array analysis showing CNN-LOH (purple line) that appears as significant dissociation in allele-specific copy number graphs (red and green lines) from the baseline with normal total copy numbers (tCN; top panel). As a result of an allelic conversion, the affected segment causes LOH (* indicates 1; bottom panel). The "acquired" origin of these lesions is indicated by the retention of substantial numbers of heterozygous SNP calls (green bars below the chromatogram) that would otherwise mostly disappear. (B) The breakpoints of 6pLOHs found in a total of 28 AA cases, all involving the HLA locus in common. In more than half of cases (indicated by arrowheads in panel B), the exact location of the breakpoint was difficult to uniquely determine, where dissociation of the allele-specific copy number graphs continuously tapered along the 6p arm, indicating the presence of multiple 6pLOH(+) clones with common missing alleles (C). Indeed, the breakpoint containing regions are separated into multiple segments having significantly different copy numbers in the circular binary segmentation model, as indicated by solid lines with *P* values. Note that the most telomeric breakpoint is located within (case 24) or centromeric to (case 23) the HLA locus in each case. (D) A skewed distribution of the logarithm of *P* values in AA cases compared with normal persons. The *P* values were calculated in the Mann-Whitney *U* test, with which the difference in the mean allele-specific copy numbers between 6p and other chromosomal regions was evaluated (see "Analysis of genomic copy numbers and detection of 6pLOH"). A total of > 250 values are plotted as 250.

HLA-A antigen; and in each case, the missing HLA-A allele was identical to that in the PB leukocytes (Figure 3B). The uniparental expression of HLA-A in case 13 was also observed in the CD34$^+$ compartment of the archived BM specimen obtained 2 years before analysis (supplemental Figure 7). Together, these findings suggested that the 6pLOH involved early HSPCs and that the 6pLOH occurred at the level of long-term repopulating stem cells.

Table 2. 6pLOH(+) AA cases and imputed allelic status of HLA alleles

UID	6pUPD(+) fraction,* %	Missing alleles						Retained alleles					
		A	B	C	DRB1	DQB1	DPB1	A	B	C	DRB1	DQB1	DPB1
19	53.9	31:01††‡	40:02†	03:04†	12:01	03:01	05:01	24:02	52:01	12:02	15:02	06:01	05:01
12	51.8	02:01††‡	40:02†	03:03	15:01	06:02	05:01	26:02	40:06	08:01	09:01	03:03	05:01
17	51.6	24:02	13:01	03:04†	12:02	03:01	04:02	24:02	52:01	12:02	15:02	06:01	09:01
304	49.3	31:01††‡	55:02	01:02	12:02	03:01	41:01	24:02	07:02	07:02	01:01	05:01	04:02
11	48.0	02:06††‡	40:02†	03:04†	15:01	06:02	ND‖	11:01	67:01	07:02	16:02	05:02	ND‖
21	46.2	31:01‡§	51:01	14:02	14:05	05:03	03:01	24:02	07:02	07:02	01:01	05:01	04:02
24	44.9	31:01†	40:02†	03:04†	11:01	03:01	02:01	24:02	40:06	08:01	09:01	03:03	05:01
26	44.3	31:01††§	40:01	03:04†	04:05	04:01	03:01	26:03	52:01	12:02	15:02	06:01	09:01
27	43.5	02:06†	40:02†	03:04†	04:10	04:02	02:01	11:01	52:01	12:02	15:02	06:01	09:01
10	42.1	31:01†	40:02†	03:04†	08:03	06:01	02:01	24:02	51:01	14:02	09:01	03:03	02:01
8	40.8	02:06††‡	40:02†	03:03	12:01	03:01	05:01	24:02	52:01	12:02	15:02	06:01	04:02
23	35.2	02:01†	40:02†	03:04†	09:01	03:03	02:01	24:02	54:01	01:02	04:05	04:01	04:02
25	32.1	02:06††‡			No LOH			01:01			No LOH		
9	23.5	02:06††‡	39:01	07:02	08:02	04:02	02:01	24:02	15:18	07:04	04:01	03:01	14:01
20	21.7	26:01‡	40:02†	03:03	15:01	06:02	05:01	02:18	46:01	01:02	08:03	06:01	05:01
14	21.7	31:01††‡	51:01	14:02	09:01	03:03	05:01	24:02	52:01	12:02	15:02	06:01	09:01
22	20.6	02:01†	39:01	07:02	08:03	06:01	05:01	24:02	52:01	12:02	15:02	06:01	09:01
18	17.6	02:01††‡	40:06	08:01	09:01	03:03	02:01	24:02	35:01	03:03	15:01	06:02	04:02
15	17.4	02:06†	40:06	08:01	09:01	03:03	02:01	24:02	07:02	07:02	01:01	05:01	02:01
41	15.2†	31:01††‡	35:01	03:03	09:01	03:03	03:01	26:01	39:01	07:02	08:03	06:01	05:01
28	12.8	24:02	54:01	01:02	01:01	05:01	04:02	24:02	52:01	12:02	15:02	06:01	09:01
29	11.7	31:01†	40:02†	03:04†	15:01	06:02	02:01	24:02	54:01	01:02	04:05	04:01	05:01
305	10.3	02:06††‡	40:02†	15:02	15:02	06:01	04:01	24:02	51:01	14:02	09:01	03:03	02:01
13	9.6	24:02‡	40:02†	03:04†	15:01	06:02	02:01	02:01‡	35:01	08:01	09:01	03:03	02:01
306	8.5	24:02‡	40:02†	03:04†	09:01	03:03	02:01	26:02	40:06	08:01	09:01	03:03	02:01
16	8.1	11:01	40:06	08:01		No LOH		24:02	46:01	01:02		No LOH	
30	8.0	02:06†	39:01	07:02		No LOH		24:02	40:06	08:01		No LOH	
72	5.6	02:01†	40:02†	03:04†	09:01	03:03	05:01	02:07	46:01	01:02	08:03	06:01	02:02
36	4.0	02:01††‡	ND¶	ND#	15:02	06:01	09:01	24:02	ND¶	ND#	15:02	06:01	09:01
124	3.5	24:02	40:02†	03:04†	12:01	03:01	02:01	24:02	52:01	12:02	15:02	06:01	09:01
223	2.8	31:01††‡	48:01	03:04†	09:01	03:03	05:01	02:06†	39:01	07:02	15:01	06:02	02:01
215	2.8	31:01†	51:01	14:02	08:02	04:02	04:02	03:01	44:02	05:01	13:01	06:03	05:01
181	1.3	02:06†	13:01	03:04†	12:02	03:01	05:01	24:02	52:01	12:02	15:02	06:01	09:01
97	1.0	24:02	07:02	07:02	01:01	05:01	05:01	02:01†	39:01	07:02	15:01	06:02	02:01
252	0.9	ND**	40:02†	03:04†	09:01	03:03	05:01	ND**	46:01	01:02	04:05	04:01	05:01
118	0.9	02:06‡§	40:02†	03:04†	08:02	03:02	05:01	24:02	52:01	12:02	15:02	06:01	09:01
298	0.8	24:02	40:02†	03:04†	15:01	06:02	05:01	24:02	52:01	12:02	15:02	06:01	09:01
188	0.7	24:02	52:01	12:02	15:02	06:01	09:01	02:01†	52:01	12:02	11:01	03:01	05:01
291	0.7	31:01†	51:01	14:02	15:01	06:02	02:01	24:02	40:01	03:04†	11:01	03:01	05:01
196	0.2	ND†† (A*02:06/24:02, B*35:01/51:01, C*03:03/15:02, DRB1*04:03/15:01, DQB1*03:02/06:02, DPB1*0:201/02:01)											

UID indicates unique ID.

*The percentage of 6pUPD(+) fraction is derived from total peripheral blood leukocytes that include lymphoid as well as myeloid element.

†HLA types significantly deviated to missing alleles.

‡The allelic loss was confirmed by flow cytometry.

§The missing haplotype was determined by flow cytometry.

‖DPB1*04:02/05:01.

¶B*15:18/52:01.

#C*08:01/12:02.

**A*02:01/02:07.

††Missing allele was not determined because copy number changes in these segments were not statistically significant.

Clonality of the HLA-missing granulocytes

The human androgen receptor-based clonality assays in granulocytes were performed in 3 6pLOH(+) and 20 6pLOH(−) patients, in which all 3 6pLOH(+) and 4 (20%) of the 6pLOH(−) patients showed evidence of clonality in granulocyte populations (supplemental Figure 8).

Missing HLA alleles in 6pLOH

Given that the HLA is the genetic target of 6pLOH in AA, the missing HLA alleles in 6pLOH are of particular interest because in this context they are thought to be directly involved in the presentation of the target auto-antigens to CTLs and, therefore, to be critically important in the pathogenesis of AA. We determined the missing HLA alleles in each 6pLOH(+) AA patient by the haplotype imputation of HLA alleles based on the large data of HLA haplotypes observed in the JMDP set, followed by statistical evaluation of allele-specific copy numbers along the imputed haplotypes (Figure 4). The imputed haplotypes were confirmed in 4 cases by the family studies on the HLA. The allelic status was imputed at least partially in 39 of the 40 6pLOH(+) cases. The imputed results were consistent with the patterns of uniparental expression of HLA-A in flow cytometry in 18 cases with 6pLOH (Table 2; Figure 4), except for those in case 26, in which no valid SNP haplotype

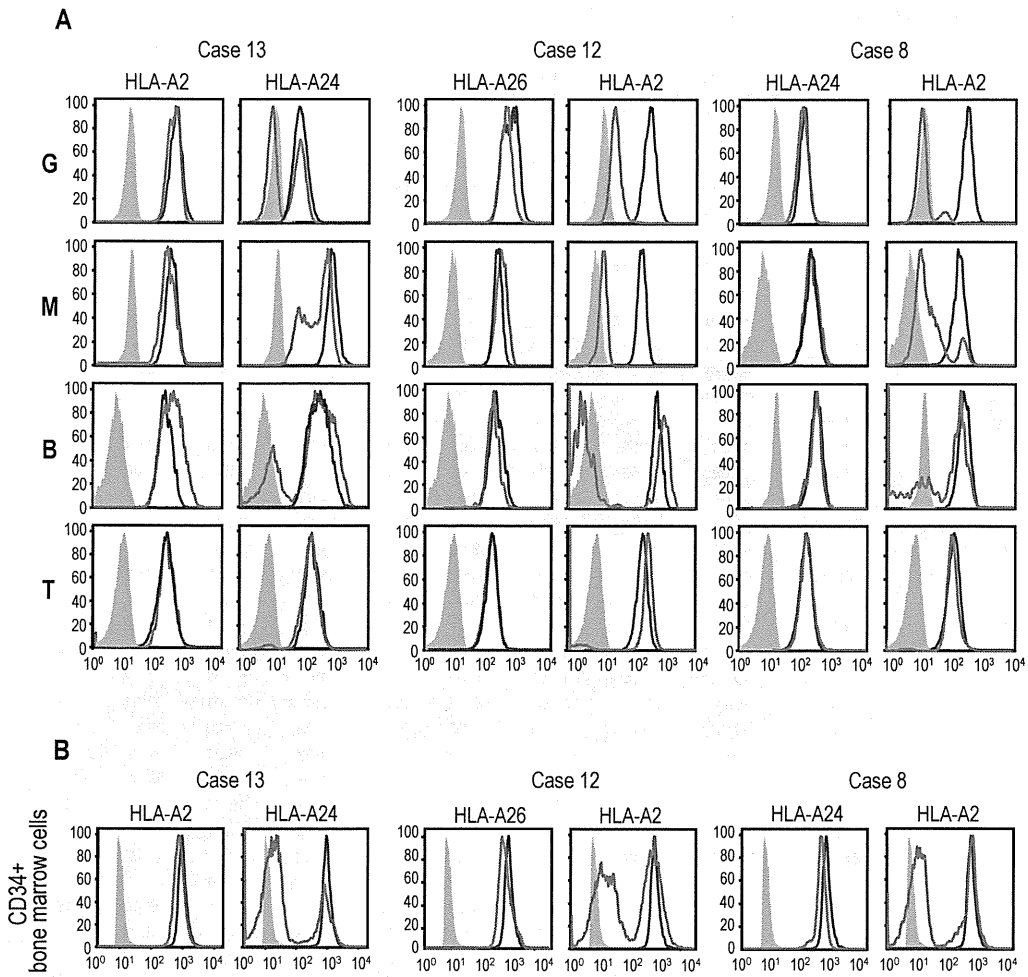

Figure 3. Uniparental expression of HLA in AA cases with CNN-LOH in 6p. Allele-specific expression of HLA-A antigens in AA specimens was examined by flow cytometry using monoclonal antibodies that specifically recognize the indicated HLA types (red lines), where leukocytes from healthy persons were used as a control (blue lines). (A-B) The uniparental expression of HLA-A antigens in PB leukocytes and BM $CD34^+$ cells obtained from 3 AA cases with CNN-LOH in 6p. Different leukocyte compartments were separately examined, including granulocytes (G), monocytes (M), B-lymphocytes (B), and T-lymphocytes (T).

around the HLA-A locus was identified and the status of HLA-A was determined by flow cytometry. The missing HLA alleles in 6pLOH(+) AA showed a conspicuous deviation to some selected HLA alleles, including HLA-A*31:01, B*40:02, C*03:04, and, to a lesser extent, HLA-A*02:01 and A*02:06. After the effects of linkage disequilibrium between individual HLA alleles were taken into consideration by multivariate analysis, 4 HLA alleles were shown to remain as the principal determinants of the missing haplotypes, HLA-A*31:01, B*40:02, A*02:01, and A*02:06 (supplemental Table 4).

Over-representation of frequently missing HLAs in AA populations

Because these missing HLA alleles in 6pLOH could be involved in the pathogenesis of AA, we next tested whether these relevant HLA alleles are associated with the risk of the development of AA among the 6,613 JMDP registrants. As shown in Table 4, the 4 major missing HLA alleles, HLA-A*31:01, B*40:02, A*02:01, and A*02:06, were more frequently observed in AA cases compared with nonsignificant HLA alleles (ie, all HLA alleles other

Table 3. Response rate (CR + PR) according to the Camitta criteria

	Newly diagnosed (n = 107)		Previously treated (n = 103)	
	6pLOH(−) (n = 91), no. (%)	6pLOH(+) (n = 16), no. (%)	6pLOH(−) (n = 88), no. (%)	6pLOH(+) (n = 15), no. (%)
Immunosuppressive therapies (all)	36/49 (73)	11/11 (100)	65/77 (84)	12/12 (100)
ATG + CsA	14/19 (74)	7/7 (100)	27/33 (82)	5/5 (100)
CsA alone	22/30 (73)	4/4 (100)	38/44 (86)	7/7 (100)
Anabolic steroid alone	0/0 (0)	0/0 (0)	7/11 (64)	2/2 (100)
Unknown/not evaluable	42	5	0	1

CR indicates complete remission; PR, partial remission; ATG, antithymocyte globulin; and CsA, cyclosporine A.

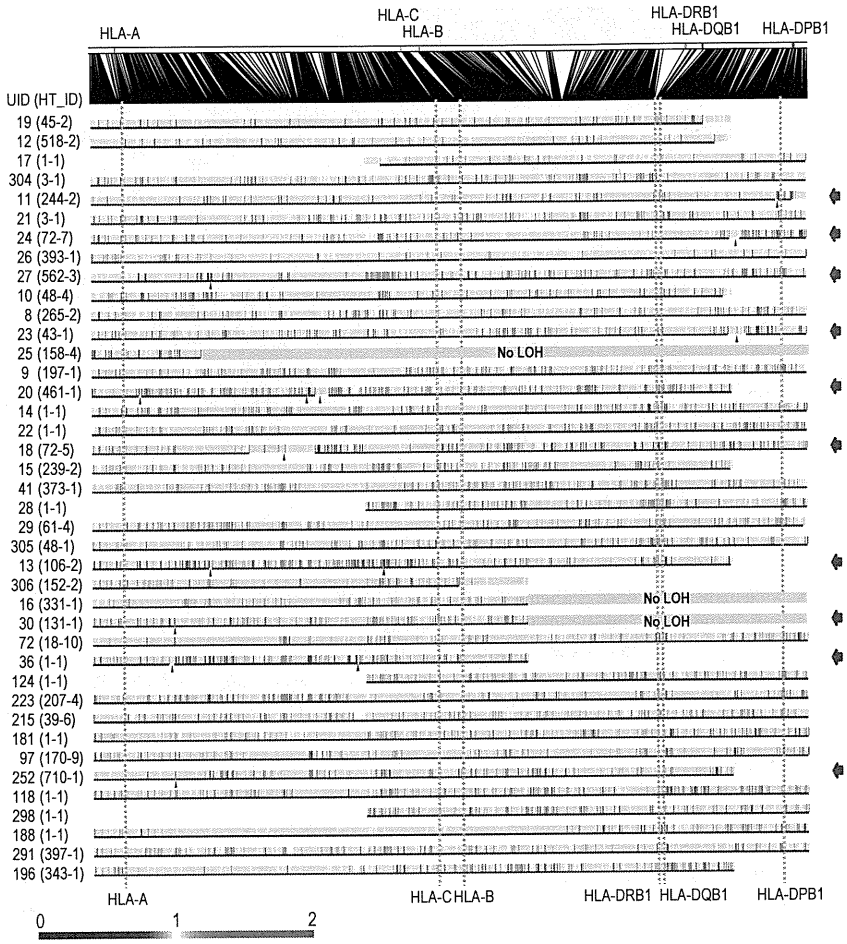

Figure 4. Imputation of missing HLA haplotypes. The observed allelic copy numbers at heterozygous SNP sites along each candidate SNP haplotype are color-coded as indicated at the bottom. Green bars showed the SNPs that are incompatible with the patient's genotype. Case IDs and haplotype ID (HT_ID) are indicated on the left. The locations of the 500K SNPs and HLA-A, C, B, DRB1, DQB1, and DPB1 are indicated in the figure. For each allele, genomic copy numbers were imputed using the circular binary segmentation algorithm. This divided each haplotype into one or more segments having discrete mean allelic copy numbers (blue arrows on the right). The positions of breakpoints are indicated by arrowheads. Finally, the mean allelic copy number of each segment was statistically compared with that of the corresponding segment on the other haplotype using the Wilcoxon signed rank test. Missing HLA haplotypes were determined based on the result of the statistic tests. Purple and blue lines indicated the retained and missing segments, respectively, whereas the allelic status was not determined statistically for those segments shown by green lines.

than these 4 alleles), where the odds ratios for the risk of the development of AA between each of these alleles and nonsignificant alleles were 1.87 (95% confidence interval [CI], 1.43-2.43) for A*02:01, 2.22 (95% CI, 1.70-2.90) for A*02:06, 1.37 (95% CI, 1.00-1.88) for A*31:01, and 1.95 (1.48-2.58) for B*40:02 (Table 4). The combined relative risk for all these alleles was 1.75 (1.42-2.17; $P = 1.3 \times 10^{-7}$).

Discussion

The origin of clonal hematopoiesis in AA is a focus of long-standing disputes, in which a profoundly reduced hematopoietic stem cell pool and/or escape from the autoimmune insults have been implicated in the evolution of the clonal hematopoiesis in AA.[5,22,23] Our findings on 6pLOH in AA provide an intriguing insight not only into the underlying mechanism of the clonal hematopoiesis in AA but also into the origin of the autoimmunity that is responsible for the pathogenesis of AA. A recent study from the United States also reported 3 cases with 6pLOH.[24] With a sensitive detection algorithm, the presence of the 6pLOH(+) components was demonstrated in as many as 13% of typical cases with AA, and the evidence from the subsequent studies strongly indicated that the HLA genes are the genetic targets of 6pLOH in AA patients. First, the HLA locus was commonly and critically involved in all 6pLOHs found in AA. Second, some AA patients carried multiple 6pLOH(+) subclones with different breakpoints, but in all cases, the 6pLOH involved the HLA locus and occurred in a manner that targeted the same parental HLA allele. Moreover, particular class I HLA alleles were over-represented among 6pLOH(+) cases and consistently found in the missing haplotypes. Finally, many of these HLA alleles were shown to be tightly

Table 4. Association of missing HLA alleles with AA in Japanese patients

Risk allele	AA (N = 407)	Other diseases (N = 6206)	Total (N = 6613)	P (χ^2 test)	Odds ratio (95% CI) (vs no risk alleles)
A*02:01	103	1173	1276	2.5×10^{-6}	1.87 (1.43–2.43)
A*02:06	100	957	1057	$< 1.0 \times 10^{-7}$	2.22 (1.70–2.90)
A*31:01	58	899	957	0.048	1.37 (1.00–1.88)
B*40:02	86	938	1024	1.8×10^{-6}	1.95 (1.48–2.58)
All risk alleles	268	3250	3518	1.3×10^{-7}	1.75 (1.42–2.17)
No risk alleles	139	2956	3095	—	—

— indicates not applicable.

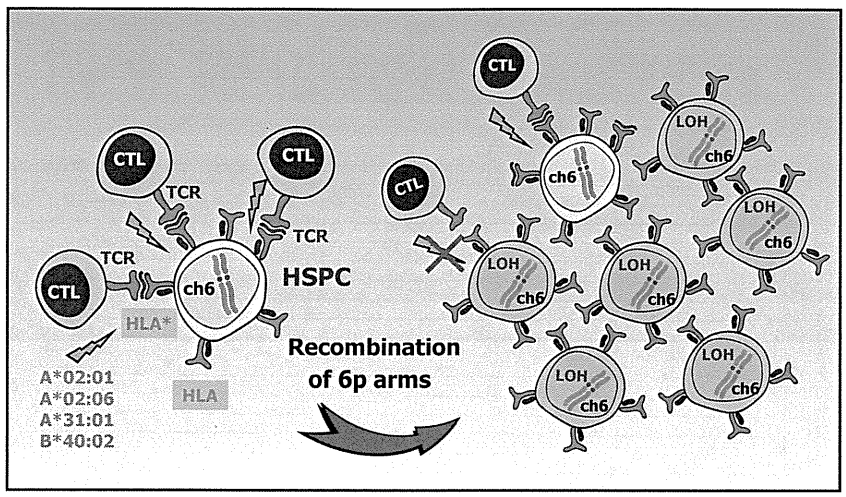

Figure 5. A proposed mechanism for escape hematopoiesis in 6pLOH(+) AA. In AA, the targets of CTLs are the HSPCs that present some auto-antigen through particular class I HLA molecules, including HLA-A*02:01, A*02:06, A*31:01, and B*40:02. In the presence of these autoimmune insults, the HSPCs that lose their expression of the antigen-presenting HLA molecule as a result of CNN-LOH in 6p would acquire a growth advantage over other HSPCs expressing the relevant HLA, leading to clonal outgrowth of the 6pLOH(+) progenies.

associated with the development of AA in Japanese patients in case-control studies using the large JMDP registry.

The conspicuous bias of the missing HLA alleles in 6pLOH to particular HLA types and the significant association of AA with those HLA types strongly suggest that the recurrent 6pLOH in AA is a phenomenon tightly related to the pathogenesis of AA rather than mere secondary event during the course of AA. Based on these observations, it is well reasoned that, in 6pLOH(+) AA cases, the autoimmunity to HSPCs is mediated by the CTLs that target the antigens presented via specific class I HLA molecules and that the 6pLOH(+) cells found in AA could be explained as escape hematopoiesis that survives the autoimmune insult by genetically deleting the relevant HLA species that are required for antigen presentation (Figure 5). These scenarios are further supported by the recent reports showing that the CNN-LOH in 6p provides a common mechanism of leukemic relapse after HLA haploidentical stem cell transplantations, in which leukemic cells that lost the mismatched HLA haplotype through CNN-LOH in 6p are thought to escape the immunologic surveillance of the engrafted donor T cells.[25,26] Importantly, it was experimentally demonstrated by immunologic assays that the 6pLOH(+) leukemic cells actually escaped GVL by CTLs, whereas 6pLOH(−) leukemic cells were effectively killed by the same CTLs. Although the immunologic targets of CTLs are different between relapse after haploidentical transplants (mismatched HLAs themselves) and AA (still unknown autoantigens presented on missing HLAs), the prominent similarities found in both cases further support that CNN-LOH in 6p confers an escape mechanism from autoreactive CTLs in AA.

In light of the above considerations, the chronologic behavior of the 6pLOH(+) components in PB is also interesting and worth discussing. Despite the assumption that 6pLOH is an effective escape mechanism from CTLs, the 6pLOH(+) stem cells were unable to repopulate the BM to cure AA, unless effective IST was applied (supplemental Figure 6). This is most probably explained by the presence of inflammatory cytokines, such as IFN-γ and TNF-α, which have also been shown to play an important role in the BM failure in AA and are thought to be responsible for the continued prevention of the 6pLOH(+) stem cells from fully expanding and reconstituting the BM (supplemental Figure 9A-B).[27,28]

When the autoimmune insults are removed after IST, no further injury of normal stem cells would occur. However, this does not necessarily mean the surviving normal stem cells can eventually outnumber the 6pLOH(+) stem cells over time. Note that, once the autoimmune insults disappear, nothing could biologically or immunologically discriminate a 6pLOH(+) stem cell from a 6pLOH(−) stem cell (supplemental Figure 9A). In particular, a 6pLOH(+) stem cell and a 6pLOH(−) stem cell will produce the same number of progeny on average and feed the same number of mature blood cells. As a consequence, once established, the predominance of 6pLOH(+) stem cells over 6pLOH(−) stem cells should be maintained, after the severely reduced hematopoietic stem cell pool has been re-expanded with removal of the inciting autoimmunity. It is also of note that the recovery of myeloid components after IST, which are affected more strongly by 6pLOH than lymphoid cells, contributes to an apparent increase in 6pLOH components in the SNP array analysis in PB (supplemental Figure 6A).

One of the most significant findings in the current study is the identification of the HLA alleles that are over-represented in the Japanese AA populations, including HLA-A*31:01, B*40:02, A*02:01, and A*02:06. All of these HLA alleles belong to class I MHCs and thus are thought to be involved in the antigen presentation to CTLs. This provides another prominent example, in which specific HLA types play a critical role in the development of a human disease, and the information about these particular HLA types provides a solid basis on which we can ultimately isolate the relevant antigens responsible for the development of AA. Of particular note, there was a previous report indicating that HLA-B*40:02 and A*02:06 were over-represented in PNH as well as AA, although the study size was much smaller than the current study.[29] Combined with our study, these findings support the hypothesis that AA and PNH are the different outcomes of the same immunologic insult[5,30] and may also provide the genetic basis of the high prevalence of AA and PNH in East Asia.[31,32]

In some AA cases, hematopoiesis could be maintained over years by the progenitors that escaped and survived the inciting autoimmune insult by deleting the target HLA through CNN-LOH in 6p. Given that the 6pLOH was detected in only 13% of our series, it is probable that other escape mechanisms may also operate to maintain hematopoiesis in AA. Indeed, clonality was clearly demonstrated in 20% of the 6pLOH(−) cases in the human androgen receptor assay study (supplemental Figure 8). In addition, our SNP array analysis also revealed a variety of clonal abnormalities in AA cases (Figure 1), although it is still open to question

whether these abnormalities actually represent the mechanism of escape hematopoiesis or were related to some neoplastic process. Further studies on the genetic basis of the escape mechanisms would contribute to our understanding of the molecular pathogenesis of AA.

Acknowledgments

The authors thank the patients and donors and their physicians, including K. Kawakami of Suzuka General Hospital and A. Okamoto of Nagoya Daini Red Cross Hospital, for contributing to this study.

This work was supported in part by the Core Research for Evolutional Science and Technology, the Japan Science and Technology Agency, the Ministry of Education, Culture, Sports, Science and Technology of Japan (Grant-in-Aids for Scientific Research), and the Ministry of Health, Labor and Welfare of Japan (Grant-in-Aids).

Authorship

Contribution: S. Ohtake, S. Ogawa, and S.N. developed the concept of the study and supervised the project; T.K., S. Ohtake, and S.N. designed the experiments; T.K., A.S.-O., Y. Sato, Y. Mori, M.K., M.S., K.H., and Y. Sasaki performed the experiments and analyzed the data; K.K. performed high-resolution HLA typing; S.M. and Y. Morishima provided the information of JMDP donor-recipient pairs (JMDP dataset); T.K., A.S.-O., S. Ogawa, and S.N. wrote the paper; and all authors approved the final version of the manuscript.

Conflict-of-interest disclosure: The authors declare no competing financial interests.

Correspondence: Shinji Nakao, Cellular Transplantation Biology, Kanazawa University Graduate School of Medical Science, 13-1 Takaramachi, Kanazawa, Ishikawa 920-8640 Japan; e-mail: snakao@med3.m.kanazawa-u.ac.jp.

References

1. Young NS, Calado RT, Scheinberg P. Current concepts in the pathophysiology and treatment of aplastic anemia. *Blood.* 2006;108(8):2509-2519.
2. Nakao S, Takami A, Takamatsu H, et al. Isolation of a T-cell clone showing HLA-DRB1*0405-restricted cytotoxicity for hematopoietic cells in a patient with aplastic anemia. *Blood.* 1997;89(10):3691-3699.
3. Chen J, Ellison FM, Eckhaus MA, et al. Minor antigen h60-mediated aplastic anemia is ameliorated by immunosuppression and the infusion of regulatory T cells. *J Immunol.* 2007;178(7):4159-4168.
4. Risitano AM, Maciejewski JP, Green S, Plasilova M, Zeng W, Young NS. In-vivo dominant immune responses in aplastic anaemia: molecular tracking of putatively pathogenetic T-cell clones by TCR beta-CDR3 sequencing. *Lancet.* 2004;364(9431):355-364.
5. Young NS. The problem of clonality in aplastic anemia: Dr Dameshek's riddle, restated. *Blood.* 1992;79(6):1385-1392.
6. Tiu R, Gondek L, O'Keefe C, Maciejewski JP. Clonality of the stem cell compartment during evolution of myelodysplastic syndromes and other bone marrow failure syndromes. *Leukemia.* 2007;21(8):1648-1657.
7. Lewis SM, Dacie JV. The aplastic anaemia-paroxysmal nocturnal haemoglobinuria syndrome. *Br J Haematol.* 1967;13(2):236-251.
8. Dameshek W. Riddle: what do aplastic anemia, paroxysmal nocturnal hemoglobinuria (PNH) and "hypoplastic" leukemia have in common? *Blood.* 1967;30(2):251-254.
9. Socie G, Rosenfeld S, Frickhofen N, Gluckman E, Tichelli A. Late clonal diseases of treated aplastic anemia. *Semin Hematol.* 2000;37(1):91-101.
10. Tichelli A, Gratwohl A, Wursch A, Nissen C, Speck B. Secondary leukemia after severe aplastic anemia. *Blut.* 1988;56(2):79-81.
11. de Planque MM, Kluin-Nelemans HC, van Krieken HJ, et al. Evolution of acquired severe aplastic anaemia to myelodysplasia and subsequent leukaemia in adults. *Br J Haematol.* 1988;70(1):55-62.
12. van Kamp H, Landegent JE, Jansen RP, Willemze R, Fibbe WE. Clonal hematopoiesis in patients with acquired aplastic anemia. *Blood.* 1991;78(12):3209-3214.
13. Kawase T, Morishima Y, Matsuo K, et al. High-risk HLA allele mismatch combinations responsible for severe acute graft-versus-host disease and implication for its molecular mechanism. *Blood.* 2007;110(7):2235-2241.
14. Nannya Y, Sanada M, Nakazaki K, et al. A robust algorithm for copy number detection using high-density oligonucleotide single nucleotide polymorphism genotyping arrays. *Cancer Res.* 2005;65(14):6071-6079.
15. Yamamoto G, Nannya Y, Kato M, et al. Highly sensitive method for genomewide detection of allelic composition in nonpaired, primary tumor specimens by use of affymetrix single-nucleotide-polymorphism genotyping microarrays. *Am J Hum Genet.* 2007;81(1):114-126.
16. Storey JD, Tibshirani R. Statistical significance for genomewide studies. *Proc Natl Acad Sci U S A.* 2003;100(16):9440-9445.
17. Ogawa S, Matsubara A, Onizuka M, et al. Exploration of the genetic basis of GVHD by genetic association studies. *Biol Blood Marrow Transplant.* 2009;15(1 suppl):39-41.
18. Morishima S, Ogawa S, Matsubara A, et al. Impact of highly conserved HLA haplotype on acute graft-versus-host disease. *Blood.* 2010;115(23):4664-4670.
19. Olshen AB, Venkatraman ES, Lucito R, Wigler M. Circular binary segmentation for the analysis of array-based DNA copy number data. *Biostatistics.* 2004;5(4):557-572.
20. Venkatraman ES, Olshen AB. A faster circular binary segmentation algorithm for the analysis of array CGH data. *Bioinformatics.* 2007;23(6):657-663.
21. Ishiyama K, Chuhjo T, Wang H, Yachie A, Omine M, Nakao S. Polyclonal hematopoiesis maintained in patients with bone marrow failure harboring a minor population of paroxysmal nocturnal hemoglobinuria-type cells. *Blood.* 2003;102(4):1211-1216.
22. Murakami Y, Kosaka H, Maeda Y, et al. Inefficient response of T lymphocytes to glycosylphosphatidylinositol anchor-negative cells: implications for paroxysmal nocturnal hemoglobinuria. *Blood.* 2002;100(12):4116-4122.
23. Bessler M, Mason PJ, Hillmen P, et al. Paroxysmal nocturnal haemoglobinuria (PNH) is caused by somatic mutations in the PIG-A gene. *EMBO J.* 1994;13(1):110-117.
24. Afable MG 2nd, Wlodarski M, Makishima H, et al. SNP array-based karyotyping: differences and similarities between aplastic anemia and hypocellular myelodysplastic syndromes. *Blood.* 2011;117(25):6876-6884.
25. Vago L, Perna SK, Zanussi M, et al. Loss of mismatched HLA in leukemia after stem-cell transplantation. *N Engl J Med.* 2009;361(5):478-488.
26. Villalobos IB, Takahashi Y, Akatsuka Y, et al. Relapse of leukemia with loss of mismatched HLA resulting from uniparental disomy after haploidentical hematopoietic stem cell transplantation. *Blood.* 2010;115(15):3158-3161.
27. Zoumbos NC, Gascon P, Djeu JY, Trost SR, Young NS. Circulating activated suppressor T lymphocytes in aplastic anemia. *N Engl J Med.* 1985;312(5):257-265.
28. Hinterberger W, Adolf G, Aichinger G, et al. Further evidence for lymphokine overproduction in severe aplastic anemia. *Blood.* 1988;72(1):266-272.
29. Shichishima T, Noji H, Ikeda K, Akutsu K, Maruyama Y. The frequency of HLA class I alleles in Japanese patients with bone marrow failure. *Haematologica.* 2006;91(6):856-857.
30. Karadimitris A, Manavalan JS, Thaler HT, et al. Abnormal T-cell repertoire is consistent with immune process underlying the pathogenesis of paroxysmal nocturnal hemoglobinuria. *Blood.* 2000;96(7):2613-2620.
31. Issaragrisil S, Kaufman DW, Anderson T, et al. The epidemiology of aplastic anemia in Thailand. *Blood.* 2006;107(4):1299-1307.
32. Montane E, Ibanez L, Vidal X, et al. Epidemiology of aplastic anemia: a prospective multicenter study. *Haematologica.* 2008;93(4):518-523.

European Journal of Haematology 86 (541–545)

CASE REPORT

Aplastic anemia successfully treated with rituximab: the possible role of aplastic anemia-associated autoantibodies as a marker for response

Hiroyuki Takamatsu[1], Hiroshi Yagasaki[2], Yoshiyuki Takahashi[3], Asahito Hama[3], Yutaka Saikawa[4], Akihiro Yachie[5], Shoichi Koizumi[6], Seiji Kojima[3], Shinji Nakao[1]

[1]Department of Hematology, School of Medicine, Institute of Medical, Pharmaceutical and Health Sciences, Kanazawa University, Kanazawa, Ishikawa, Japan; [2]Department of Pediatrics, School of Medicine, Nihon University, Itabashi-ku, Tokyo, Japan; [3]Department of Pediatrics, Nagoya University Graduate School of Medicine, Nagoya, Aichi, Japan; [4]Department of Pediatrics, Kanazawa Medical University, Uchinada, Ishikawa, Japan; [5]Department of Pediatrics, School of Medicine, Institute of Medical, Pharmaceutical and Health Sciences, Kanazawa University, Kanazawa, Ishikawa, Japan; [6]Research Center for Child Mental Development, Kanazawa University, Kanazawa, Ishikawa, Japan

Abstract

A 1-yr-old Japanese male infant developed hepatitis-associated aplastic anemia (AA), and anti-thymocyte globulin (ATG) plus cyclosporine A (CsA) was administered without any appreciable effects. Laboratory examination of the patient's serum obtained before therapy revealed various autoantibodies, such as PA-IgG, anti-platelets, anti-single-stranded DNA (ssDNA), and anti-double-stranded DNA (dsDNA) antibodies (Abs) in addition to anti-DRS-1 Abs and anti-moesin Abs, both of which are known to be detectable in approximately 40% of all patients presenting with AA. He was therefore treated with 17.5 mg/kg/d rituximab 5.5 months after ATG/CsA therapy. The same rituximab therapy was repeated three times once a month thereafter. His neutrophil counts started to increase 50 d after the first rituximab therapy and he achieved a complete remission at 16 months after the last rituximab administration. All of the autoantibodies including anti-ssDNA, dsDNA, DRS-1, and moesin became undetectable when he attained the remission. Anti-CD20 monoclonal antibody therapy may be effective in a subset of patients with AA characterized by the presence of autoantibodies.

Key words aplastic anemia; rituximab; autoantibody

Correspondence Hiroyuki Takamatsu, MD, PhD, Department of Hematology, School of Medicine, Institute of Medical, Pharmaceutical and Health Sciences, Kanazawa University, 13-1 Takaramachi, Kanazawa, Ishikawa 920-8641, Japan. Tel: +81 76 265 2273; Fax: +81 76 234 4252; e-mail: takamaz@med3.m.kanazawa-u.ac.jp

Accepted for publication 20 March 2011

doi:10.1111/j.1600-0609.2011.01612.x

Rituximab, a chimeric human/mouse monoclonal antibody targeting the CD20 antigen, has been successfully used for treatments of various autoimmune hematologic diseases such as immune thrombocytopenic purpura (ITP), autoimmune hemolytic anemia (AIHA), and thrombotic thrombocytopenic purpura (TTP) (1–6). In this case report, we describe a child with aplastic anemia (AA) who failed to respond to a first course of anti-thymocyte globulin (ATG) plus cyclosporine A (CsA) therapy but later improved with rituximab treatment. To our knowledge, this is the first pediatric AA case that was successfully treated with rituximab.

Method

Detection of anti-DRS-1 and anti-moesin autoantibodies by Western blotting analysis

Approximately 5 μg of recombinant native DRS-1 or moesin protein per lane was electrophoresed in a 12% polyacrylamide gel and transferred to a PVDF membrane. The membrane was incubated in 3% BSA–PBS containing serum diluted 1 : 200 from this AA patient or a healthy individual (7, 8).

Case report

A 15-month-old Japanese male infant was admitted to a nearby hospital because of a high fever and intraoral bleeding in February of 2006. He was born to healthy non-consanguineous parents and was normally nourished. The family history did not include hematologic or malignant diseases. Physical examination on admission showed petechiae and no splenomegaly, and the liver was palpable 2 cm below the right costal arch. His complete blood count (CBC) showed a red blood cell (RBC) count of 3.71×10^{12}/L and hemoglobin (Hb) level of 11.0 g/dL. A white blood cell (WBC) count of 21.3×10^{9}/L with a differential count of eosinophils 0%, basophils 0%, neutrophils 50%, lymphocytes 47%, and monocytes 3%, and a platelet count of 9.0×10^{9}/L. Bone marrow (BM) aspiration and biopsy showed a slight hypoplasia with relatively reduced granulocytes. No signs of myelodysplasia or an increase in the number of atypical cells were observed. The G-banding of 20 metaphase BM cells showed all cells to be a normal karyotype, 46, XY. No Abs specific to viruses were found, including the hepatitis A virus, hepatitis B virus, hepatitis C virus, Epstein–Barr virus, or parvovirus B19, other than anti-cytomegalovirus IgG Abs. Autoantibody screening revealed the presence of Abs against smooth muscle, cardiolipin, single-stranded DNA (ssDNA), double-stranded DNA (dsDNA), SS-A, SS-B, Sm, platelets, and PA-IgG. Anti-liver/kidney microsome type 1 Abs were of a borderline titer, but all of antinuclear Abs, rheumatoid factor, and anti-neutrophil Abs were negative. The haptoglobin level was within the normal range. Blood chemistry revealed abnormal values as follows: IgG 2035 mg/dL (normal range 820–1740 mg/dL), AST 203 IU/L (normal range 10–40 IU/L), ALT 609 IU/L (normal range 5–40 IU/L), LDH 304 IU/L (normal range 115–210 IU/L), ALP 838 IU/L (normal range 104–338 IU/L), and T-bil 1.3 mg/dL (normal range 0.2–1.0 mg/dL). A contrast-enhanced CT study of the patient's abdomen was normal. He was diagnosed to have autoimmune hepatitis (AIH) with ITP. Bolus methylprednisolone (250 mg/d for 3 d) followed by prednisolone (2 mg/kg/d) and high-dose IVIG (0.4 g/kg/d) for 5 d were administered from March 18, 2006. His AIH resolved in 4 wk but pancytopenia further progressed, necessitating frequent RBC and platelet transfusion. On June 29, 2006, a CBC showed a RBC count of 2.47×10^{12}/L and Hb 7.5 g/dL, a reticulocyte count of 8.0×10^{9}/L, a WBC count of 2.3×10^{9}/L with eosinophils 1%, basophils 0%, neutrophils 6%, lymphocytes 92%, monocytes 1%, a neutrophil count of 0.1×10^{9}/L, and a platelet count of 58×10^{9}/L. BM aspiration and biopsy showed a severe hypocellularity with fatty change. The G-banding of seven metaphase BM cells showed all cells to have a normal karyotype, 46, XY. Very severe AA was diagnosed (Fig. 1A). Abs specific to DRS-1 and moesin, which are detectable in approximately 40% of patients with AA (7, 8), were positive in the serum of this patient. No increase in the glycophosphatidylinositol-anchored protein–deficient erythrocytes and granulocytes was observed. On July 5, 2006, ATG (Lymphoglobuline; Aventis Behring, King of Prussia, PA; 15 mg/[kg/d], 5 d) plus cyclosporine (CsA, 4–12 mg/[kg/d]; Novartis, Basel, Switzerland) was administered according to the standard protocol (9), but no increases in blood cells count were observed 5.5 months later (Fig. 1B). HLA-identical donors were unavailable from the Japan Marrow Donor Program either. Because the patient was positive for various autoantibodies, the effect of anti-B-cell therapy was anticipated. Therefore, 17.5 mg/kg/d of rituximab was started from December 19 of 2006, 5.5 months after ATG therapy. A CBC showed a RBC count of 2.33×10^{12}/L and Hb 6.5 g/dL, a reticulocyte count of 4.0×10^{9}/L, a WBC count of 2.0×10^{9}/L, a neutrophil count of 0.2×10^{9}/L and a platelet count of 53×10^{9}/L at the time of the first rituximab administration. Written informed consent was obtained from his parents prior to the treatment. The same dose of rituximab

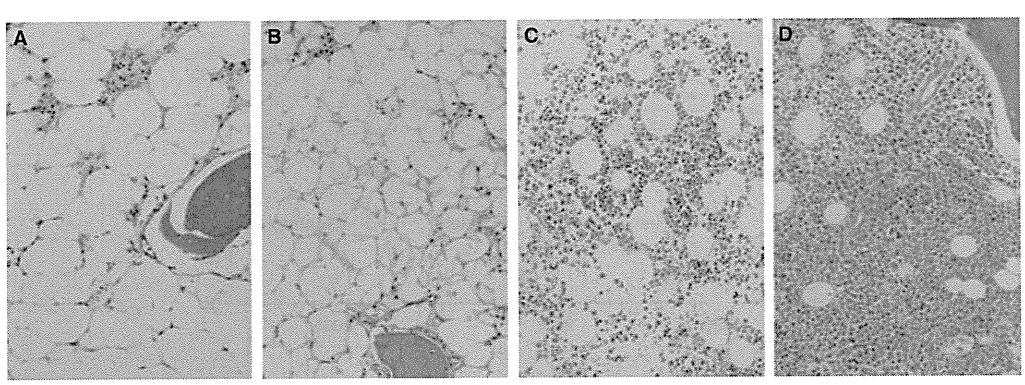

Figure 1 Changes in the bone marrow cellularity associated with rituximab. (A) before therapy; (B) 2 months after anti-thymocyte globulin/cyclosporine A (ATG/CsA) therapy; (C) 10 months after the first rituximab therapy; (D) 22 months after the first rituximab therapy.

was given monthly four times, and 80 mg/d CsA was continued. The neutrophil count of the patient started to rise 50 d after the first rituximab administration and then continued to rise thereafter. Twenty months after the first rituximab therapy, his neutrophil was more than 5.0×10^9/L, the Hb level 11 g/dL, and the platelet count 158×10^9/L (Fig. 2). A BM biopsy performed at 10 months of the first rituximab therapy showed myeloid and erythroid hyperplasia with reduced megakaryopoiesis (Fig. 1C), and another BM biopsy performed at 22 months of the therapy revealed a hypercellularity of all three lineage of cells (Fig. 1D). Abs against ssDNA, dsDNA, SS-A, SS-B, Sm, DRS-1, and moesin became undetectable in August of 2008 (Fig. 2), and the titers of PA-IgG and anti-cardiolipin Abs were reduced from 142.9 to 71.1 ng/10^7cells and from 39.1 to 17.9 U/mL, respectively. From January to March in 2008, the patient had fever and inflammatory bowel disease of unknown etiology. Severe thrombocytopenia recurred after high-dose IVIG (0.3 g/kg/d) was administered to treat the bowel disease. A BM biopsy revealed abundant megakaryocytes suggestive of thrombocytopenia because of increased platelet destruction secondary to IVIG therapy (Fig. 2). Four years after the rituximab therapy, his CBC was normal, and his AA was in complete remission (CR) as of October of 2010.

Discussion

Immune-mediated suppression or destruction of hematopoietic stem cells is a major mechanism implicated in the pathophysiology of AA (10–12), where aberrant T-cell responses to autoantigens lead to excessive production of various cytokines, including interferon-γ (IFN-γ) and tumor necrosis factor-α (TNF-α) in the BM (13–15). Immunosuppression with ATG and/or CsA targeting autoreactive T cells has been successfully applied to resolve such immune-mediated AA (16–18). Antibody-mediated stem cell insults may also be responsible for BM failure in some patients with AA, but only one case of adult AA, which responded to rituximab, has been reported (19).

Rituximab is thought to induce a remission of autoimmune cytopenias such as ITP, AIHA, and TTP by eliminating circulating $CD20^+$ B cells including B cells capable of producing autoantibodies. Rituximab also has an indirect effect on cellular immunity (6, 20). The elimination of $CD20^+$ B cells may indirectly normalize abnormalities in the cellular immunity of patients with ITP such as T-cell receptor Vβ skewing, a decrease in both the T-helper cell type 1 (Th1)/Th2 ratio and the Fas ligand expression on Th1 and Th2 cells, and also the regulatory T-cell number (21, 22). Increases in regulatory T cells have been reported after rituximab treatment of patients with systemic lupus erythematosus (23, 24).

Recent studies identified several autoantibodies against kinectin (25), postmeiotic segregation increased one (26), DRS-1 (7), moesin (8), and hnRNPk (27) in the sera of patients with AA. Among these autoantibodies, Abs against moesin, an intracellular protein that links the cell membrane and cytoskeleton, are unique in the way that they can enhance the secretion of TNF-α and INF-γ from PBMCs of AA patients through the activation of the ERK1/2 pathway that is provoked by direct binding to moesin on the cells (28, 29). This suggests that the elimination of such functional autoantibodies by rituximab therapy may restore hematopoiesis in AA patients

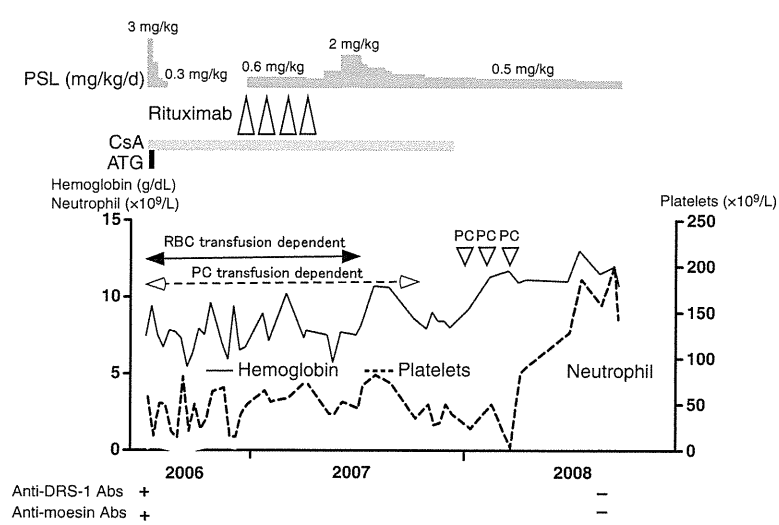

Figure 2 Clinical course after immunosuppressive therapy. PC, platelet concentrate; PSL, prednisolone; +, positive; −, negative. The black solid line and gray solid line indicate hemoglobin and the absolute neutrophil count, respectively. The dotted line indicates the platelet count.

by way of abolishing the excessive secretion of TNF-α and IFN-γ.

Some AA patients who failed to respond to ATG/CsA within 6 months of the therapy conversely showed a late response and thereby eventually achieved transfusion independence (18). It therefore cannot be denied that the CR obtained after rituximab therapy was induced by ATG/CsA. However, our patient did not show any signs of hematologic improvement, such as an increase in the platelet or reticulocytes count at the time of the rituximab administration, which was day 168 of the ATG therapy. His neutrophil, reticulocyte, and platelet count began to increase on days 50, 158, and 309 of the first rituximab therapy, respectively. Given the fact that it takes several weeks until the titer of pathogenic autoantibodies sufficiently decreases after rituximab administration, it seems more reasonable to ascribe the hematologic recovery to the effect of rituximab than to the late effect of ATG. The disappearance of AA-associated autoantibodies including anti-DRS-1 Abs and anti-moesin Abs after rituximab supports the role of rituximab in the restoration of the patient's marrow failure.

In conclusion, we herein presented the first case where rituximab was successfully used as an alternative treatment for a pediatric patient with severe AA who was refractory to standard ATG/CsA therapy. The presence of autoantibodies such as anti-DRS-1 Abs and anti-moesin Abs may be useful for predicting response to rituximab therapy in AA patients. The results of this case warrant a clinical trial using rituximab for the treatment of patients with AA refractory to ATG.

Acknowledgements

We thank the medical staff of Department of Pediatrics, Kanazawa University, and Department of Pediatrics, Nagoya University, for providing excellent therapy for this patient and for providing his clinical information. We also thank Dr Zhirong Qi of Cellular Transplantation Biology of Kanazawa University for technical assistance. This work was supported by a Grant-in-Aid for Scientific Research from the Ministry of Education, Science, Technology, Sports, and Culture of Japan (KAKENHI 21591237).

Conflict of interest

The authors declare no conflict of interest.

References

1. Zecca M, Nobili B, Ramenghi U, *et al.* Rituximab for the treatment of refractory autoimmune hemolytic anemia in children. *Blood* 2003;**101**:3857–61.
2. Arnold DM, Dentali F, Crowther MA, Meyer RM, Cook RJ, Sigouin C, Fraser GA, Lim W, Kelton JG. Systematic review: efficacy and safety of rituximab for adults with idiopathic thrombocytopenic purpura. *Ann Intern Med* 2007;**146**:25–33.
3. Scully M, Cohen H, Cavenagh J, Benjamin S, Starke R, Killick S, Mackie I, Machin SJ. Remission in acute refractory and relapsing thrombotic thrombocytopenic purpura following rituximab is associated with a reduction in IgG antibodies to ADAMTS-13. *Br J Haematol* 2007;**136**:451–61.
4. Godeau B, Porcher R, Fain O, *et al.* Rituximab efficacy and safety in adult splenectomy candidates with chronic immune thrombocytopenic purpura: results of a prospective multicenter phase 2 study. *Blood* 2008;**112**:999–1004.
5. Michel M, Chanet V, Dechartres A, *et al.* The spectrum of Evans syndrome in adults: new insight into the disease based on the analysis of 68 cases. *Blood* 2009;**114**:3167–72.
6. Stasi R. Rituximab in autoimmune hematologic diseases: not just a matter of B cells. *Semin Hematol* 2010;**47**:170–9.
7. Feng X, Chuhjo T, Sugimori C, Kotani T, Lu X, Takami A, Takamatsu H, Yamazaki H, Nakao S. Diazepam-binding inhibitor-related protein 1: a candidate autoantigen in acquired aplastic anemia patients harboring a minor population of paroxysmal nocturnal hemoglobinuria-type cells. *Blood* 2004;**104**:2425–31.
8. Takamatsu H, Feng X, Chuhjo T, Lu X, Sugimori C, Okawa K, Yamamoto M, Iseki S, Nakao S. Specific antibodies to moesin, a membrane-cytoskeleton linker protein, are frequently detected in patients with acquired aplastic anemia. *Blood* 2007;**109**:2514–20.
9. Kojima S, Hibi S, Kosaka Y, Yamamoto M, Tsuchida M, Mugishima H, Sugita K, Yabe H, Ohara A, Tsukimoto I. Immunosuppressive therapy using antithymocyte globulin, cyclosporine, and danazol with or without human granulocyte colony-stimulating factor in children with acquired aplastic anemia. *Blood* 2000;**96**:2049–54.
10. Viale M, Merli A, Bacigalupo A. Analysis at the clonal level of T-cell phenotype and functions in severe aplastic anemia patients. *Blood* 1991;**78**:1268–74.
11. Zoumbos NC, Gascon P, Djeu JY, Trost SR, Young NS. Circulating activated suppressor T lymphocytes in aplastic anemia. *N Engl J Med* 1985;**312**:257–65.
12. Herrmann F, Griffin JD, Meuer SG, Meyer zum Buschenfelde KH. Establishment of an interleukin 2-dependent T cell line derived from a patient with severe aplastic anemia, which inhibits in vitro hematopoiesis. *J Immunol* 1986;**136**:1629–34.
13. Young NS. Hematopoietic cell destruction by immune mechanisms in acquired aplastic anemia. *Semin Hematol* 2000;**37**:3–14.
14. Hara T, Ando K, Tsurumi H, Moriwaki H. Excessive production of tumor necrosis factor-alpha by bone marrow T lymphocytes is essential in causing bone marrow failure in patients with aplastic anemia. *Eur J Haematol* 2004;**73**:10–6.

15. Dubey S, Shukla P, Nityanand S. Expression of interferon-gamma and tumor necrosis factor-alpha in bone marrow T cells and their levels in bone marrow plasma in patients with aplastic anemia. *Ann Hematol* 2005;**84**:572–7.
16. Bacigalupo A, Broccia G, Corda G, *et al.* Antilymphocyte globulin, cyclosporin, and granulocyte colony-stimulating factor in patients with acquired severe aplastic anemia (SAA): a pilot study of the EBMT SAA Working Party. *Blood* 1995;**85**:1348–53.
17. Rosenfeld SJ, Kimball J, Vining D, Young NS. Intensive immunosuppression with antithymocyte globulin and cyclosporine as treatment for severe acquired aplastic anemia. *Blood* 1995;**85**:3058–65.
18. Frickhofen N, Heimpel H, Kaltwasser JP, Schrezenmeier H. Antithymocyte globulin with or without cyclosporin A: 11-year follow-up of a randomized trial comparing treatments of aplastic anemia. *Blood* 2003;**101**:1236–42.
19. Hansen PB, Lauritzen AM. Aplastic anemia successfully treated with rituximab. *Am J Hematol* 2005;**80**:292–4.
20. Cooper N, Arnold DM. The effect of rituximab on humoral and cell mediated immunity and infection in the treatment of autoimmune diseases. *Br J Haematol* 2010;**149**:3–13.
21. Stasi R, Del Poeta G, Stipa E, Evangelista ML, Trawinska MM, Cooper N, Amadori S. Response to B-cell depleting therapy with rituximab reverts the abnormalities of T-cell subsets in patients with idiopathic thrombocytopenic purpura. *Blood* 2007;**110**:2924–30.
22. Stasi R, Cooper N, Del Poeta G, Stipa E, Laura Evangelista M, Abruzzese E, Amadori S. Analysis of regulatory T-cell changes in patients with idiopathic thrombocytopenic purpura receiving B cell-depleting therapy with rituximab. *Blood* 2008;**112**:1147–50.
23. Sfikakis PP, Souliotis VL, Fragiadaki KG, Moutsopoulos HM, Boletis JN, Theofilopoulos AN. Increased expression of the FoxP3 functional marker of regulatory T cells following B cell depletion with rituximab in patients with lupus nephritis. *Clin Immunol* 2007;**123**:66–73.
24. Vallerskog T, Gunnarsson I, Widhe M, Risselada A, Klareskog L, van Vollenhoven R, Malmstrom V, Trollmo C. Treatment with rituximab affects both the cellular and the humoral arm of the immune system in patients with SLE. *Clin Immunol* 2007;**122**:62–74.
25. Hirano N, Butler MO, Von Bergwelt-Baildon MS, Maecker B, Schultze JL, O'Connor KC, Schur PH, Kojima S, Guinan EC, Nadler LM. Autoantibodies frequently detected in patients with aplastic anemia. *Blood* 2003;**102**:4567–75.
26. Hirano N, Butler MO, Guinan EC, Nadler LM, Kojima S. Presence of anti-kinectin and anti-PMS1 antibodies in Japanese aplastic anaemia patients. *Br J Haematol* 2005;**128**:221–3.
27. Qi Z, Takamatsu H, Espinoza JL, Lu X, Sugimori N, Yamazaki H, Okawa K, Nakao S. Autoantibodies specific to hnRNP K: a new diagnostic marker for immune pathophysiology in aplastic anemia. *Ann Hematol* 2010;**89**:1255–63.
28. Espinoza JL, Takamatsu H, Lu X, Qi Z, Nakao S. Anti-moesin antibodies derived from patients with aplastic anemia stimulate monocytic cells to secrete TNF-alpha through an ERK1/2-dependent pathway. *Int Immunol* 2009;**21**:913–23.
29. Takamatsu H, Espinoza JL, Lu X, Qi Z, Okawa K, Nakao S. Anti-moesin antibodies in the serum of patients with aplastic anemia stimulate peripheral blood mononuclear cells to secrete TNF-alpha and IFN-gamma. *J Immunol* 2009;**182**:703–10.

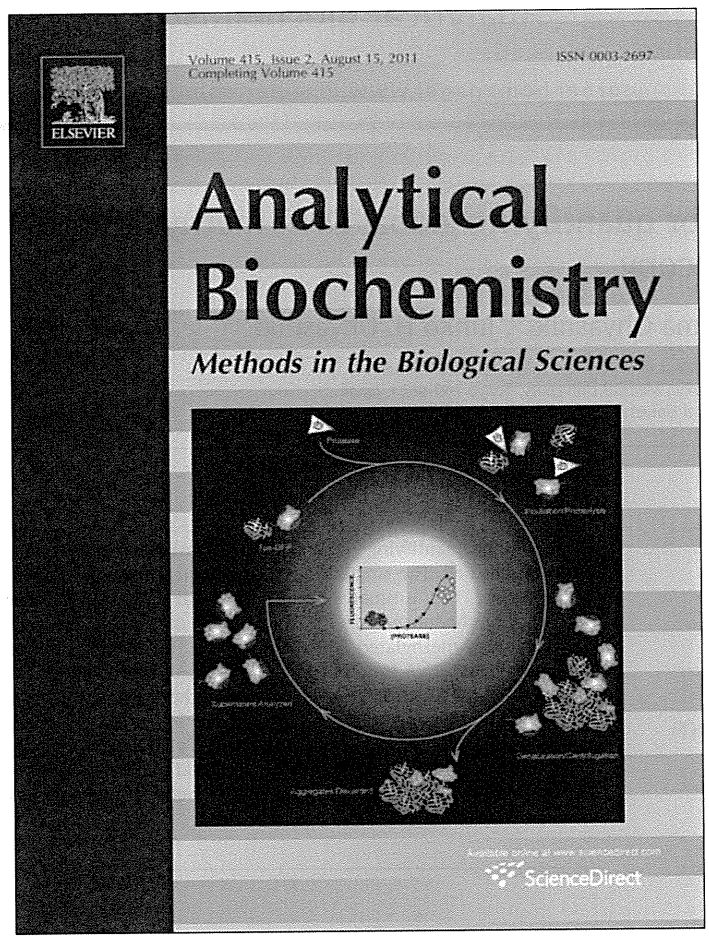

Analytical Biochemistry 415 (2011) 145–150

Contents lists available at ScienceDirect

Analytical Biochemistry

journal homepage: www.elsevier.com/locate/yabio

Detection method for quantifying global DNA methylation by fluorescence correlation spectroscopy

Tomohiro Umezu [a], Kazuma Ohyashiki [b], Junko H. Ohyashiki [c,*]

[a] Department of Molecular Science, Tokyo Medical University, Tokyo 160-0023, Japan
[b] First Department of Internal Medicine, Tokyo Medical University, Tokyo 160-0023, Japan
[c] Institute of Medical Science, Tokyo Medical University, Tokyo 160-0023, Japan

ARTICLE INFO

Article history:
Received 28 January 2011
Received in revised form 16 April 2011
Accepted 21 April 2011
Available online 27 April 2011

Keywords:
Methyl-CpG-binding domain (MBD)
Fluorescence correlation spectroscopy (FCS)
Global DNA methylation

ABSTRACT

A method for quantifying global DNA methylation using fluorescence correlation spectroscopy (FCS) has been established. The single-molecule methylation assay (SMMA) is based on two methodologies. One methodology, FCS, estimates the translational diffusion coefficient of molecules in solution, whereas the other methodology uses the high affinity of methyl-CpG-binding domain protein 2 (MBD2) to bind specifically to methylated DNA. We studied the specific binding rates of fluorescence-labeled MBD2 and methylated DNA from biological samples using the automated FCS system. Using a standard curve with methylated control DNA, we developed the SMMA index to assess the global DNA methylation level of the biological samples. A marked decrease in the SMMA index was observed when human leukemia cell lines (U937 and K562) were cultured with DNA demethylating agents. Our findings clearly indicate the applicability of SMMA as a simple and rapid tool for quantifying global DNA methylation. SMMA may prove useful for genome-wide comparative methylation analyses of malignancies and as an indicator of the demethylation effects of epigenetic drugs.

Genomic DNA methylation plays an important role both during normal cell development and in tumorigenesis. The methylation occurs almost exclusively in CpG dinucleotides. Although the CpG dinucleotides constitute only 1% of the human genome, CpG-rich stretches, so-called CpG islands, are located in the promoter regions of more than 70% of all known human genes [1–3]. In normal cells, CpG islands are unmethylated, reflecting a transcriptionally active state of the respective genes. Epigenetic silencing of tumor suppressor genes by hypermethylation of CpG islands is a very early and stable characteristic of tumorigenesis [4–6]. In contrast, global DNA hypomethylation seems to occur in early neoplasia and is a feature of genomic DNA derived from solid tumor tissues; such hypomethylation leads to chromosomal instability and increased tumor frequency, as well as oncogene activation [7,8]. Accordingly, aberrant methylation patterns, either global DNA hypomethylation or hypermethylation of tumor suppressor genes, are considered a hallmark of human cancers.

Methyl-CpG-binding protein appears to be the central player in the process of DNA methylation-dependent gene silencing. MeCP2, MBD1, MBD2, MBD3, and MBD4 compose a family of nuclear proteins, each of which contains a methyl-CpG-binding domain (MBD).[1] Each of these proteins is capable of binding specifically to a single symmetrically methylated CpG pair in any sequence context and of recruiting chromatin remodeling and transcriptional repressor complexes, thereby establishing a repressive chromatin state [9]. The MBD has been used to separate and purify the methylated DNA in methylation analyses such as CpG island microarray and methyl-CpG immunoprecipitation [10].

Here we describe a new method for quantifying global DNA methylation using fluorescence correlation spectroscopy (FCS) and the high affinity of MBD for methylated DNA. The single-molecule methylation assay (SMMA) is based on fluorescence colocalization imaging of two single molecules, fluorescence-labeled MBD and methylated DNA (Fig. 1). The concept of FCS was developed more than 30 years ago [11,12], and with recent advances in laser and microscopic technologies, it now has single-molecule sensitivity. FCS measures fluorescence intensity fluctuations of fluorescently labeled molecules that, as a result of Brownian motion in a solution, cross through the immobile confocal region formed by a laser. The translational diffusion time in which a

* Corresponding author. Address: Institute of Medical Science (Oncology Division), Tokyo Medical University, 6-7-1 Nishi-shinjuku, Shinjuku, Tokyo 160-0023, Japan. Fax: +81 3 3345 0185.
E-mail addresses: t_umezu@tokyo-med.ac.jp (T. Umezu), ohyashik@rr.iij4u.or.jp (K. Ohyashiki), junko@hh.iij4u.or.jp (J.H. Ohyashiki).

[1] *Abbreviations used:* 5-AzaC, 5-azacytidine; DAC, 5-aza-2′-deoxycytidine; FCS, fluorescence correlation spectroscopy; MBD, methyl-CpG-binding domain; SMMA, single-molecule methylation assay; TAMRA-MBD2, TAMRA-labeled MBD2.

0003-2697/$ - see front matter © 2011 Elsevier Inc. All rights reserved.
doi:10.1016/j.ab.2011.04.035

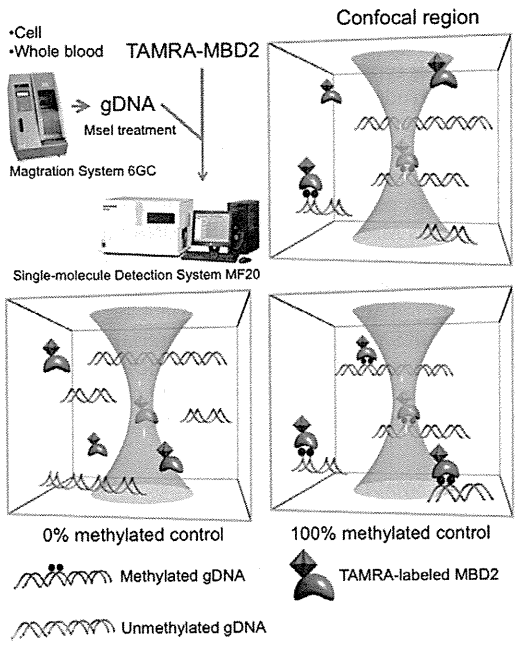

Fig.1. Schematic diagram of the SMMA method. The confocal region formed by the laser is depicted by the green area; genomic DNA fragment is represented by a spiral line; methylated CpG is represented by black spheres; recombinant MBD2 is depicted by a blue shape; nonexcited TAMRA is represented by a black octahedron; and excited TAMRA is a pink octahedron. Genomic DNA was purified with the robotic workstation (Magtration System 6GC, Precision System Science), and the crude genomic DNA was fragmented with MseI. Using the automated FCS system (MF20, Olympus), we measured the changes in diffusion time of TAMRA-MBD2. To quantify the binding of TAMRA-MBD2 with methylated DNA, we used FCS to analyze the binding of TAMRA-MBD2 with whole genome amplification (WGA) control DNA (0% methylated) or M.SssI-treated DNA (100% methylated). (For interpretation of the references to color in this figure legend, the reader is referred to the web version of this article.)

molecule stays in the focal volume depends on its hydrodynamic radius. Recently, DNA–DNA interactions [13], DNA–RNA interactions, and protein–protein interactions [14,15] have been analyzed by FCS. Therefore, FCS is ideally suited for analyzing specific interactions [16] and single-nucleotide polymorphism (SNP) [17]. Our findings clearly indicate the applicability of FCS as a reliable, simple, and rapid tool for quantifying the binding of TAMRA-labeled MBD2 (TAMRA-MBD2) with methylated DNA.

With SMMA, the difference in diffusion time of TAMRA-MBD2, resulting from methylated DNA binding, could be quantified, and the specificity of the binding was shown even in crude biological samples. The SMMA technique may prove useful for genome-wide comparative methylation analyses of malignancies and as an indicator of the demethylation effects of epigenetic drugs.

Materials and methods

Cell culture

The human leukemia cell lines U937 and K562 were cultured in RPMI 1640 supplemented with 10% heat-inactivated fetal bovine serum, penicillin (100 U/ml), and streptomycin (100 mg/ml) at 37 °C in a humidified atmosphere of 95% air–5% CO_2. For demethylation experiments, U937 and K562 cells, 5×10^5 each, were grown for 72 h with 3 μM 5-azacytidine (5-AzaC) (Sigma, St. Louis, MO, USA) or 5 μM 5-aza-2′-deoxycytidine (Decitabine, DAC; Wako, Osaka, Japan). The DNA demethylating agents were replenished each day.

Purification and preparation of genomic DNA

Purification of genomic DNA was performed with the robotic workstation (Magtration System 6GC, Precision System Science, Chiba, Japan), for automated purification of nucleic acids, and with the EZ1 DNA Blood 350 μl kit (Qiagen, Valencia, CA, USA) according to the manufacturer's instructions. For each subject, at least 500 ng of genomic DNA was digested with MseI (New England Biolabs, Beverly, MA, USA). Completion of the digest was confirmed with agarose gel electrophoresis, and the digested DNA was quantified with NanoDrop ND-1000 (Thermo Fisher Scientific, Waltham, MA, USA).

CpG unmethylated or methylated control DNA

To generate CpG-unmethylated DNA (0% methylated control), we amplified human control DNA (Qiagen) using the REPLI-g mini kit (Qiagen) according to the manufacturer's instructions. Briefly, amplification was carried out in two steps. The step 1 reaction mixture contained 5–10 ng of DNA in 1 μl of sterile water and 9 μl of sample buffer. This mixture was heated at 95 °C for 3 min and then chilled on ice. Step 1 resulted in denaturation of the genomic DNA template. The step 2 reaction (amplification) mixture contained 9 μl of reaction buffer, 1 μl of enzyme mix, and 10 μl of the product from step 1. The amplification reaction was incubated at 30 °C for 16–18 h. Step 2 allows binding of the exonuclease-resistant random hexamers and subsequent isothermal amplification. The enzyme was inactivated by heating at 65 °C for 10 min, followed by cooling to 4 °C. The reaction was purified with the QIAquick PCR purification kit (Qiagen).

We generated CpG-methylated DNA (100% methylated control) by methylating CpG motifs within the whole genome amplification (WGA) DNA using the CpG methylase M.SssI kit (New England Biolabs) according to the manufacturer's instructions. Briefly, 1.5 μg of WGA DNA was combined with 2 μl of 10× NEBuffer 2, 0.1 μl of *S*-adenosylmethionine, 5 units of M.SssI, and sterile water up to a final volume of 20 μl. The reaction was incubated at 37 °C for 4 h and then purified with the QIAquick PCR purification kit (Qiagen). The DNA concentration was determined with a NanoDrop ND-1000 spectrophotometer.

Bisulfite genomic sequencing

Genomic DNA was chemically modified with EpiTect Bisulfite Kits (Qiagen), a treatment that changes the unmethylated but not the methylated cytosine into uracil. Bisulfite-treated DNA was subjected to polymerase chain reaction (PCR) amplification with the use of primers designed to recognize both methylated and unmethylated forms of the *p16/INK4a* promoter region: p16-F: 5′-GAGGAGGGGTTGGTTGGTTATTAGAG-3′ and p16-R: 5′-TACCTA ATTCCAATTCCCCTACAAAC-3′, and the *p15/INK4b* promoter region: p15-F: 5′-TGGGGATTAGGAGCTGAGGG-3′ and p15-R: 5′-TCTGGCA GAGTGGGGAGCCAGCC-3′. The resulting PCR products were fractionated in low-melting agarose (Sigma), purified with the QIAEX II kit (Qiagen), and cloned into the pGEM-T Easy vector (Promega, Madison, WI, USA). DNA of individual clones was then sequenced with an ABI Prism 3130xl Genetic Analyzer (Applied Biosystems, Foster City, CA, USA).

Preparation of TAMRA-labeled MBD2

Fluorescently labeled and unlabeled MBD2 was purchased from Protein Express, Inc. (Chiba, Japan). The procedures for protein expression and purification of MBD2 domain were described in previous reports [18,19]. Using the pROX–FL vector included in the coding sequence of MBD2, we synthesized TAMRA-labeled

MBD2 with an RTS 100 *Escherichia coli* HY kit (Roche Diagnostics, Basel, Switzerland) and the TAMRA-tRNA (TAMRA-X aminophenylalanyl-$tRNA_{cccg}$) included in the In vitro Pin-point fluorescence labeling kit 543 (Olympus, Tokyo, Japan). The reaction mixture for in vitro translation (150 μl) contained 15 μl of the plasmid DNA (100 ng/μl), 15 μl of TAMRA-tRNA, 36 μl of amino acid, 3 μl of methionine, 30 μl of reaction mix, and 36 μl of *E. coli* lysate. Amino acids, methionine, reaction mix, and 36 μl of *E. coli* lysate were included in the RTS 100 *E. coli* HY kit. The reaction mixture was incubated at 30 °C for 2 h. Expressed TAMRA-labeled substrates were purified with His Spin Trap columns (GE Healthcare, Piscataway, NJ, USA) according to the supplier's instructions. Substrates were concentrated with an UltraFree-0.5 centrifuge (Millipore, Bedford, MA, USA), and the substrate sizes and concentrations were confirmed by sodium dodecyl sulfate–polyacrylamide gel electrophoresis.

Binding reaction of DNA and TAMRA-labeled MBD2

TAMRA-MBD2 (5 nM) was incubated at room temperature for 20 min with 10 ng DNA (MseI-treated gDNA) in 40 μl of 50 mM Tris buffer (pH 7.5) containing 70 mM KCl, 1 mM EDTA, 1 mM 2-mercaptoethanol, 0.2 mg/ml bovine serum albumin, and 4% glycerol. For competition analysis, 0–500 nM unlabeled MBD2 (WT-MBD2) was incubated with 10 ng of methylated control DNA (100% methylated control) for 20 min prior to the addition of TAMRA-MBD2.

FCS measurements

The MF20 single-molecule fluorescence detection system (Olympus) was used for FCS measurements. Each 35-μl sample was added to a 384-well glass-bottomed microplate. These samples were sequentially and automatically loaded into the device, the optical system of which was also automatically adjusted for each measurement. For the detection of TAMRA-MBD2, a He–Ne laser (543 nm) and 580DF30 filter were used. All experiments were performed under identical conditions with a data acquisition time of 5 s per measurement, and measurements were repeated 15 times per sample. A cutoff at chi square distribution of >600 was set to improve the reproducibility of the mean value of 15 measurements. The standard deviations of diffusion times were calculated from the average values of the three tests for each sample.

Statistical analysis

We used GraphPad Prism 5.0 software (GraphPad Software Inc., San Diego, CA, USA) for statistical analysis. A Mann–Whitney test was used to determine statistical significances between the control and test groups. *P* values less than 0.05 were considered to indicate statistically significant differences.

Results

Detection of MBD2-genomic DNA complex by FCS analysis

The schematic chart of the SMMA procedure is shown in Fig. 1. We assumed that recombinant MBD2 could be used to discriminate methylated and unmethylated DNA in crude biological samples [20–23]. First, genomic DNA was purified with the robotic workstation (Magtration System 6GC, Precision System Science), and the crude genomic DNA was fragmented with MseI. After mixing fragmented DNA and TAMRA-MBD2, we measured the changes in diffusion time of TAMRA-MBD2 using the automated FCS system (MF20, Olympus). Thus, the binding of TAMRA-MBD2 with methylated DNA can be quantified simply and rapidly.

To explore this type of application at the single-molecular level, we fragmented crude genomic DNA with MseI, which was chosen because it is known to preferentially cleave in regions of low CpG content while leaving many CpG islands intact. The electrophoretic images of MseI-treated genomic DNA are shown in Fig. 2. The intact genomic DNA purified from U937 cells was larger than 8 kbp (Fig. 2A), whereas MseI cleaved genomic DNA into fragments that were spread densely from 200 to 1000 bp (Fig. 2B). Using the automated FCS system, we measured the diffusion time that TAMRA-MBD2 was reacted with MseI-treated DNA or nontreated DNA (see Tables S1 and S2 in Supplementary material). The 15 measurements were inconsistent when TAMRA-MBD2 was reacted with nontreated DNA, whereas the reproducibility of repeated measurements was confirmed with MseI-treated DNA.

Definition of the SMMA index

With the use of the standard curve for methylated control DNA, the diffusion time can be converted into percentage values to assess the global DNA methylation level of sample DNA. First, to generate the methylated control DNA, we performed WGA and M.SssI treatments. When WGA control DNA of the *p15/INK4b* and the *p16/INK4a* promoter regions was analyzed by bisulfite sequencing, all CpGs were demethylated. In contrast, all CpGs were methylated in M.SssI-treated DNA of the *p15/INK4b* and the *p16/INK4a* promoter regions (Fig. 3A).

Next, the binding of TAMRA-MBD2 with methylated DNA was examined by using 0% and 100% methylated control DNA (Fig. 3B). We used different concentrations of control DNA (0–40 ng) and measured the changes in diffusion time of TAMRA-MBD2. The diffusion time of unbound free TAMRA-MBD2 was determined as 697.2 ± 8.4 μs. When 100% methylated control DNA was added, a dose-dependent prolongation of the diffusion time, resulting from the formation of an MBD2-methylated DNA complex, was observed (Fig. 3B, solid bars). These binding reactions appeared to be saturated in the presence of <40 ng methyl-

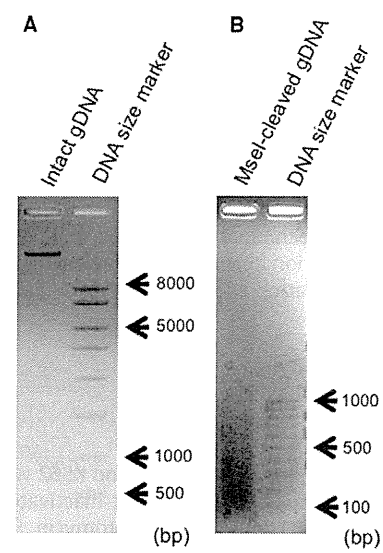

Fig.2. The electrophoretic images of MseI-treated genomic DNA. For each subject, at least 500 ng of genomic DNA was digested with MseI. Completion of the digest was confirmed with agarose gel electrophoresis. (A) The intact genomic DNA purified from U937 cells was larger than 8 kbp. (B) MseI cleaved genomic DNA into fragments that were spread densely from 200 to 1000 bp. The right lanes in (A) and (B) indicate the DNA size marker.

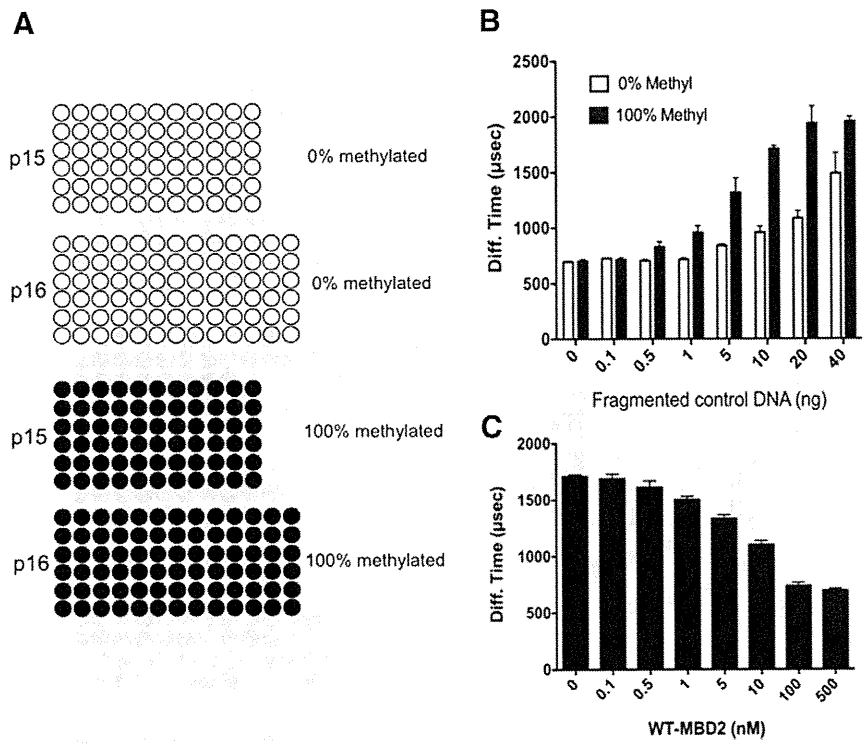

Fig.3. Detection of MBD2-methylated genomic DNA complex by FCS analysis. To generate control DNA to quantify the binding of TAMRA-MBD2 with methylated genomic DNA, we performed WGA and M.SssI treatment. (A) Bisulfite sequencing results of the WGA-treated (0% methylated control) and M.SssI-treated (100% methylated control) genomic DNA of the *p15/INK4b* and the *p16/INK4a* promoter regions. Each circle indicates a CpG site in the primary sequence, and each line of circles represents analysis of a single cloned allele. Open and closed circles represent unmethylated and methylated C residues, respectively. (B) The relationship between diffusion time and genomic DNA contents. TAMRA-MBD2 was incubated at room temperature for 20 min with MseI-treated control DNA (0, 0.1, 0.5, 1, 5, 10, 20, or 40 ng). The concentration of TAMRA-MBD2 was fixed at 5 nM. Closed bars indicate the diffusion time of TAMRA-MBD2 with 100% methylated control DNA. Open bars indicate the diffusion time of TAMRA-MBD2 with 0% methylated control DNA. Values represent the mean ± SD of three tests. (C) MBD2 competition assay for specificity of methylated DNA binding. Different concentrations (0–100 nM) of unlabeled MBD2 (WT-MBD2) were incubated with 100% methylated control DNA (10 ng) for 20 min prior to the addition of TAMRA-MBD2 (5 nM). Values represent the mean ± SD of 3 tests. Diff., diffusion.

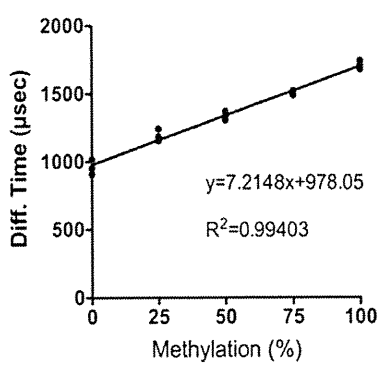

Fig.4. Establishment of standard curve for the SMMA index. The binding of TAMRA-MBD2 with 0% methyl control (WGA-treated DNA/M.SssI-treated DNA proportions of 4:0), 25% methyl control (WGA-treated DNA/M.SssI-treated DNA proportions of 3:1), 50% methyl control (WGA-treated DNA/M.SssI-treated DNA proportions of 2:2), 75% methyl control (WGA-treated DNA/M.SssI-treated DNA proportions of 1:3), and 100% methyl control (WGA-treated DNA/M.SssI-treated DNA proportions of 0:4) were analyzed by FCS. Diff., diffusion.

ated DNA. On the other hand, unspecific binding between MBD2 and unmethylated DNA increased in a manner dependent on the concentration of 0% methyl control DNA (Fig. 3B, open bars). Thus, to further detect the specificity of the binding reaction between MBD2 and methylated DNA, the density of DNA used to react with MBD2 was fixed to 10 ng.

We next estimated the specificity of the binding reaction between MBD2 and methylated DNA by competition assay, in which an excess amount of unlabeled MBD2 (WT-MBD2) was added to the reaction mixture of TAMRA-MBD2 and 100% methylated control DNA. The binding of 100% methylated DNA (10 ng) with TAMRA-MBD2 (5 nM) was completely blocked in the presence of more than a 20-fold amount of WT-MBD2 (100 nM) (Fig. 3C). These results indicate that the binding of TAMRA-MBD2 with methylated DNA was a sequence-specific interaction.

We next tried to establish the standard curve for quantifying global DNA methylation of crude biological samples. A series of mixtures of WGA-treated control DNA (0% methylated control) and M.SssI-treated control DNA (100% methylated control) in diluted proportions of 4:0, 3:1, 2:2, 1:3, and 0:4 was used. Fig. 4 shows the standard curve that can measure global DNA methylation status. As shown in this figure, a linear relationship was found ($y = 7.2148x + 978.05$, $R^2 = 0.99403$). The linear correlation shows that measurements of the percentages of global DNA methylation (0%, 25%, 50%, 75%, and 100%) are well distinguished and can be used to determine an SMMA index for test samples.

SMMA index of genome methylation in leukemia cell lines treated with DNA demethylating agents

We used the SMMA index to attempt to quantify the demethylation effect of DNA demethylating agents. U937 and K562 cells were grown for 72 h with 3 μM 5-AzaC or 5 μM DAC, and the crude genomic DNA was collected and fragmented with MseI. The binding of TAMRA-MBD2 with MseI-treated genomic DNA was analyzed by FCS, and the diffusion time was converted to the SMMA

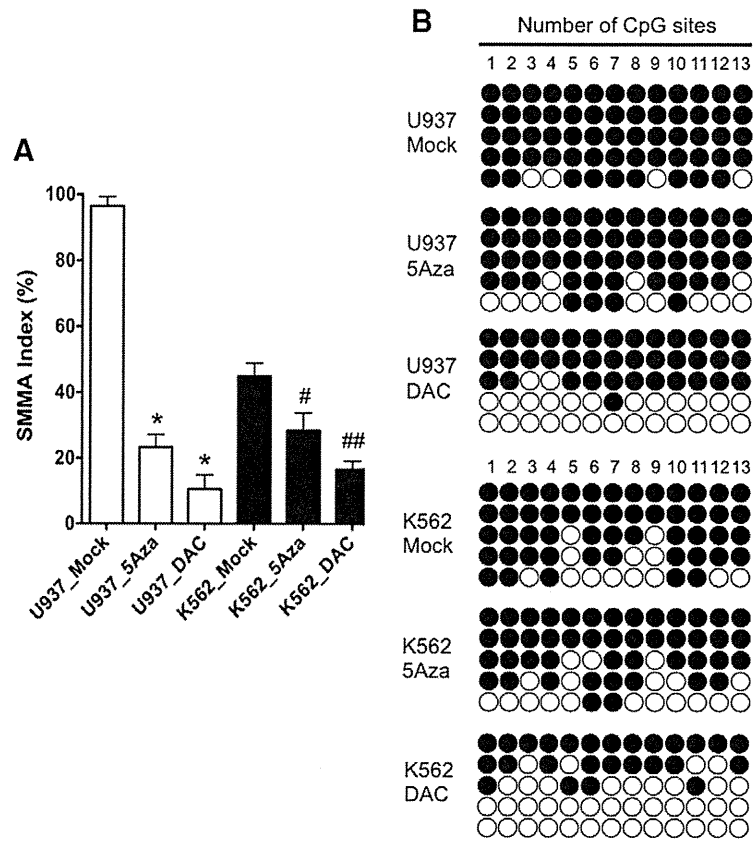

Fig.5. Quantification of the demethylation effect of DNA demethylating agents. For demethylation experiments, U937 and K562 cells were grown for 72 h with 3 μM 5-AzaC or 5 μM DAC. (A) Diffusion times of DNA methylation in cell lines treated with DNA demethylating agents. The binding of TAMRA-MBD2 with MseI-treated genomic DNA was analyzed by FCS. Demethylation effects by 5-AzaC and DAC: open bars indicate diffusion time of the 5-AzaC- or DAC-treated U937 cells; solid bars indicate diffusion time of the 5-AzaC- or DAC-treated K567 cells. Values represent the mean ± SD of three tests. $^{*}P < 0.0001$ versus U937_Mock. $^{\#}P = 0.0432$ versus K562_Mock. $^{\#\#}P < 0.01$ versus K562_Mock. (B) Bisulfite sequencing results of the p16/INK4a promoter in U937 and K562 cells cultured for 72 h with 3 μM 5-AzaC or 5 μM DAC. Each circle indicates a CpG site in the primary sequence, and each line of circles represents analysis of a single cloned allele. Open and closed circles represent unmethylated and methylated C residues, respectively.

index. The SMMA index decreased significantly in the 5-AzaC- or DAC-treated U937 cells compared with mock cells ($P < 0.0001$, Fig. 5A, open bar, and Table S3). We found a modest decrease in the SMMA index in 5-AzaC-treated K562 cells; however, no significant change was seen because of the originally low SMMA index (Fig. 5A, solid bar and Table S3).

Furthermore, to compare the SMMA method, we measured the demethylation effect of DNA demethylating agents using a currently available method. The genomic DNA derived from 5-AzaC- and DAC-treated U937 and K562 cells of the *p16/INK4a* promoter region was analyzed by bisulfite sequencing (promoter-associated analysis). As shown in Fig. 5B, the *p16/INK4a* promoter is highly methylated in U937 cells (94%) and K562 cells (80%). When cells were treated with DAC, the methylation level decreased to 58% in U937 cells and to 40% in K562 cells. However, no significant change was seen in the 5-AzaC-treated cells (82% in U937 cells and 71% in K562 cells), suggesting that the demethylation effect of 5-AzaC differed between the SMMA method (genome-wide analysis) and the bisulfite sequencing method (promoter-associated analysis).

Discussion

We have established a novel approach to quantitatively determine the global DNA methylation levels using FCS, namely the SMMA method. This method provides an alternative method for evaluating global DNA methylation with a small amount of input DNA. This study clearly indicates the applicability of SMMA as a robust, simple, and fast tool for quantifying the global DNA methylation level in biological samples, such as genomic DNA extracted from human cells.

Global DNA methylation can be detected with bisulfite conversion, methylation-sensitive restriction enzymes, methyl-binding proteins, and anti-methylcytosine antibodies [24,25]. However, the results obtained using techniques based on these principles likely will be biased, because the procedures are complicated. In contrast, SMMA using the FCS technique is less time consuming, and the measurements can be carried out within 1–2 min per sample. Thus, an assay based on FCS could facilitate the analysis of DNA–protein interactions tens of times faster than previous methods; the total assay time is only 4 h. Moreover, no primary modification of genomic DNA is needed, and the assay requires only 500 ng of genomic DNA.

Members of the MBD protein family bind to methylated DNA by recognizing methylated cytosines, and they regulate protein biosynthesis by recruitment of transcriptional repression complexes to silence gene expression. SMMA is based on the selective enrichment of methylated DNA fragments by fluorescently labeled MBD2. The binding of MBD2 to methylated DNA is relatively sequence independent, in contrast to other methylated CpG-binding proteins (MeCP2, MBD3, and MBD4) [20,21,24]. In human colon

cancer, the *p14/ARF* and *p16/INK4a* tumor suppressor genes are commonly inactivated by MBD2-mediated aberrant methylation of their promoter regions [26]. Moreover, a deficiency of MBD2 strongly inhibits intestinal tumorigenesis in the Min mouse, suggesting that the protein might be involved in transcriptional repression of methylated tumor suppressor genes [22]. Therefore, while it is logical that we choose MBD2 as the fluorescently labeled molecule, unfortunately, we did not have a chance to compare MBD2 with other fluorescently labeled methylated CpG-binding proteins.

DNA methylation is a reversible epigenetic process [27], which makes it an attractive potential therapeutic target of cancer. The only approved way to target DNA methylation is to inhibit the DNMT enzymes. DNMT inhibitors that are clinically available and indicated for myelodysplastic syndrome (MDS) include 5-AzaC and DAC [27]. Although both 5-AzaC and DAC show clinical response to MDS, it is unknown to what extent the clinical activity of DNMT inhibitors depends on reversal of methylation, or if a clinical response can be detected by reversal of methylation early in the course of treatment. In the current study, we compared the DNA demethylation effects induced by 5-AazC and DAC in U937 cells, using both genome-wide analysis by SMMA and conventional methylation analysis of *p16/INK4a* by bisulfite sequencing. With conventional methylation analysis, we failed to detect the effect of demethylation of a single gene; however, we found a marked demethylation effect in 5-AzaC-treated U937 cells by SMMA. These findings strongly suggest that the effect of demethylating agents on genomic methylation cannot be judged from an assessment of limited regions.

Although we could not simply compare the results obtained with the SMMA method and a genome-wide methylation array that contains promoter-associated CpG islands, we found a similar drug-dependent decrease of methylation in both assays (Fig. S1). This indicates that the global DNA methylation level could be more useful than the methylation of single promoter-associated CpG sites to estimate the demethylation status in human cells, especially in patient samples with heterogeneous methylation profiles.

In conclusion, our results show that SMMA might be a robust and simple method for quantifying the level of global genome methylation, even if the source of the DNA is crude cellular extracts. SMMA may be useful for genome-wide comparative methylation analyses of clinical samples (e.g., cancer tissue versus noncancer tissue, patients versus healthy subjects, drug-treated patients versus treatment-naïve patients). Taken together, our results indicate that SMMA is a powerful method for studying global genome methylation in molecular biological and clinical research.

Acknowledgments

This work was supported by the "Promotion of Science and Technology" project for private universities, with a matching fund subsidy from the Ministry of Education, Culture, Sports, Science, and Technology (MEXT), 2009–2014, and by the "University-Industry Joint Research Project" for private universities with a matching fund subsidy from MEXT, 2007–2009. Thanks are also due to Dr. N. Kato (Olympus Corp.) for her advice, and Ms. C. Kobayashi, R. Soya-Hamamura, A. Hirota, and Mr. Y. Kamimura for their technical assistance.

Appendix A. Supplementary data

Supplementary data associated with this article can be found, in the online version, at doi:10.1016/j.ab.2011.04.035.

References

[1] R.L. Momparler, Cancer epigenetics, Oncogene 22 (2003) 6479–6483.
[2] C. Plass, Cancer epigenomics, Hum. Mol. Genet. 11 (2002) 2479–2488.
[3] A.G. Tsai, H. Lu, S.C. Raghavan, M. Muschen, C.L. Hsieh, M.R. Lieber, Human chromosomal translocations at CpG sites and a theoretical basis for their lineage and stage specificity, Cell 135 (2008) 1130–1142.
[4] E.E. Cameron, S.B. Baylin, J.G. Herman, p15(INK4B) CpG island methylation in primary acute leukemia is heterogeneous and suggests density as a critical factor for transcriptional silencing, Blood 94 (1999) 2445–2451.
[5] P.A. Jones, P.W. Laird, Cancer epigenetics comes of age, Nat. Genet. 21 (1999) 163–167.
[6] C.L. Hsieh, Dependence of transcriptional repression on CpG methylation density, Mol. Cell. Biol. 14 (1994) 5487–5494.
[7] P.A. Jones, S.B. Baylin, The fundamental role of epigenetic events in cancer, Nat. Rev. Genet. 3 (2002) 415–428.
[8] M. Ehrlich, Cancer-linked DNA hypomethylation and its relationship to hypermethylation, Curr. Top. Microbiol. Immunol. 310 (2006) 251–274.
[9] E. Ballestar, A.P. Wolffe, Methyl-CpG-binding proteins. Targeting specific gene repression, Eur. J. Biochem. 268 (2001) 1–6.
[10] E. Ballestar, M.F. Paz, L. Valle, S. Wei, M.F. Fraga, J. Espada, J.C. Cigudosa, T.H. Huang, M. Esteller, Methyl-CpG binding proteins identify novel sites of epigenetic inactivation in human cancer, EMBO J. 22 (2003) 6335–6345.
[11] M. Ehrenberg, E. Cronvall, R. Rigler, Fluorescence of proteins interacting with nucleic acids. Correction for light absorption, FEBS Lett. 18 (1971) 199–203.
[12] D. Magde, E.L. Elson, W.W. Webb, Fluorescence correlation spectroscopy. II. An experimental realization, Biopolymers 13 (1974) 29–61.
[13] M. Kinjo, R. Rigler, Ultrasensitive hybridization analysis using fluorescence correlation spectroscopy, Nucleic Acids Res. 23 (1995) 1795–1799.
[14] K. Kuroki, S. Kobayashi, M. Shiroishi, M. Kajikawa, N. Okamoto, D. Kohda, K. Maenaka, Detection of weak ligand interactions of leukocyte Ig-like receptor B1 by fluorescence correlation spectroscopy, J. Immunol. Methods 320 (2007) 172–176.
[15] G. Maertens, J. Vercammen, Z. Debyser, Y. Engelborghs, Measuring protein–protein interactions inside living cells using single color fluorescence correlation spectroscopy. Application to human immunodeficiency virus type 1 integrase and LEDGF/p75, FASEB J. 19 (2005) 1039–1041.
[16] M. Eigen, R. Rigler, Sorting single molecules: application to diagnostics and evolutionary biotechnology, Proc. Natl. Acad. Sci. USA 91 (1994) 5740–5747.
[17] M. Bannai, K. Higuchi, T. Akesaka, M. Furukawa, M. Yamaoka, K. Sato, K. Tokunaga, Single-nucleotide-polymorphism genotyping for whole-genome-amplified samples using automated fluorescence correlation spectroscopy, Anal. Biochem. 327 (2004) 215–221.
[18] H. Nakata, T. Ohtsuki, M. Sisido, A protease inhibitor discovery method using fluorescence correlation spectroscopy with position-specific labeled protein substrates, Anal. Biochem. 390 (2009) 121–125.
[19] R. Abe, K. Shiraga, S. Ebisu, H. Takagi, T. Hohsaka, Incorporation of fluorescent non-natural amino acids into N-terminal tag of proteins in cell-free translation and its dependence on position and neighboring codons, J. Biosci. Bioeng. 110 (2010) 32–38.
[20] J. Berger, A. Bird, Role of MBD2 in gene regulation and tumorigenesis, Biochem. Soc. Trans. 33 (2005) 1537–1540.
[21] M. Fodermayr, J. Proll, O. Zach, C. Wechselberger, D. Lutz, In vitro detection of methylated DNA via recombinant protein MBD2b, Mol. Biol. Rep. 36 (2009) 1859–1862.
[22] O.J. Sansom, J. Berger, S.M. Bishop, B. Hendrich, A. Bird, A.R. Clarke, Deficiency of Mbd2 suppresses intestinal tumorigenesis, Nat. Genet. 34 (2003) 145–147.
[23] P.A. Wade, Methyl CpG-binding proteins and transcriptional repression, Bioessays 23 (2001) 1131–1137.
[24] T.A. Rauch, G.P. Pfeifer, The MIRA method for DNA methylation analysis, Methods Mol. Biol. 507 (2009) 65–75.
[25] M. Karimi, S. Johansson, T.J. Ekstrom, Using LUMA: a luminometric-based assay for global DNA-methylation, Epigenetics 1 (2006) 45–48.
[26] V. Martin, H.F. Jorgensen, A.S. Chaubert, J. Berger, H. Barr, P. Shaw, A. Bird, P. Chaubert, MBD2-mediated transcriptional repression of the p14ARF tumor suppressor gene in human colon cancer cells, Pathobiology 75 (2008) 281–287.
[27] J.G. Herman, S.B. Baylin, Gene silencing in cancer in association with promoter hypermethylation, N. Engl. J. Med. 349 (2003) 2042–2054.

Leukemia (2011) 25, 110–120

www.nature.com/leu

ORIGINAL ARTICLE

Impact of adjunct cytogenetic abnormalities for prognostic stratification in patients with myelodysplastic syndrome and deletion 5q

M Mallo[1,2,3,12], J Cervera[1,3,12], J Schanz[4], E Such[1,3], G García-Manero[5], E Luño[1,3], C Steidl[4], B Espinet[1], T Vallespí[1,3,6], U Germing[4], S Blum[7], K Ohyashiki[8,9], J Grau[1,3], M Pfeilstöcker[4], JM Hernández[1,3], T Noesslinger[4], A Giagounidis[4], C Aul[4], MJ Calasanz[1,3], ML Martín[1,3], P Valent[10], R Collado[1,3], C Haferlach[9,11], C Fonatsch[4], M Lübbert[4], R Stauder[4], B Hildebrandt[4], O Krieger[4], C Pedro[3], L Arenillas[3], MÁ Sanz[3], A Valencia[1,3], L Florensa[3], GF Sanz[3,13], D Haase[4,9,13] and F Solé[1,2,3,9,13]

[1]Spanish Haematological Cytogenetics Working Group, Spain; [2]Faculty of Life Sciences, Department of Cell Biology, Physiology, and Immunology, Autonomous University of Barcelona, Bellaterra, Spain; [3]Spanish MDS Registry Group, Spain; [4]German–Austrian MDS Study Group, Germany and Austria; [5]Department of Leukemia, The University of Texas MD Anderson Cancer Center, Houston, USA; [6]International Working Group on Morphology of MDS (MDS Foundation); [7]Hematology Service, University Hospital Vaudois, Lausanne, Switzerland; [8]Division of Hematology, The First Department of Internal Medicine, Tokyo Medical University, Tokyo, Japan; [9]International Working Group on MDS Cytogenetics (MDS Foundation); [10]Department of Medicine I, Medical University of Vienna, Vienna, Austria and [11]Munich Leukemia Laboratory, Munich, Germany

This cooperative study assessed prognostic factors for overall survival (OS) and risk of transformation to acute myeloid leukemia (AML) in 541 patients with *de novo* myelodysplastic syndrome (MDS) and deletion 5q. Additional chromosomal abnormalities were strongly related to different patients' characteristics. In multivariate analysis, the most important predictors of both OS and AML transformation risk were number of chromosomal abnormalities ($P<0.001$ for both outcomes), platelet count ($P<0.001$ and $P=0.001$, respectively) and proportion of bone marrow blasts ($P<0.001$ and $P=0.016$, respectively). The number of chromosomal abnormalities defined three risk categories for AML transformation (del(5q), del(5q)+1 and del(5q)+ ⩾2 abnormalities) and two for OS (one group: del(5q) and del(5q)+1; and del(5q)+ ⩾2 abnormalities, as the other one); with a median survival time of 58.0 and 6.8 months, respectively. Platelet count ($P=0.001$) and age ($P=0.034$) predicted OS in patients with '5q−syndrome'. This study demonstrates the importance of additional chromosomal abnormalities in MDS patients with deletion 5q, challenges the current '5q−syndrome' definition and constitutes a useful reference series to properly analyze the results of clinical trials in these patients.
Leukemia (2011) **25,** 110–120; doi:10.1038/leu.2010.231; published online 30 September 2010
Keywords: '5q−syndrome'; cytogenetics; deletion 5q; myelodysplastic syndromes

Introduction

Myelodysplastic syndromes (MDS) are a group of clonal hematopoietic stem cell diseases characterized by dysplasia and ineffective hematopoiesis in one or more myeloid cell lines. MDS is associated with a variable overall survival (OS) and a relatively high risk of progression to acute myeloid leukemia (AML). Evolution to AML and the clinical consequences of cytopenias are main causes of morbidity and mortality in MDS.[1–3]

Correspondence: Dr F Solé, Laboratori de Citogenètica Molecular, Servei de Patologia, Hospital del Mar, Passeig Marítim, 25-29, 08003 Barcelona, Spain.
E-mail: fsole@parcdesalutmar.cat
[12]These authors equally contributed to this work.
[13]These authors equally contributed to the coordination of the project.
Received 29 April 2010; revised 11 August 2010; accepted 26 August 2010; published online 30 September 2010

Although many specific chromosomal abnormalities have been associated with MDS, partial or complete deletion of the long arm of chromosome 5 (deletion 5q), with or without additional karyotypic abnormalities, is present in 10–15% of patients with *de novo* MDS, and thus is the most frequently documented recurrent cytogenetic abnormality in MDS.[4–8] Outcomes among MDS patients with deletion 5q vary greatly, both in terms of OS and risk of transformation to AML.[5,8–11] The presence of additional chromosomal abnormalities or an excess of blasts shortens OS and increases the risk of AML transformation.[5,8,10,11] The '5q−syndrome' is the only MDS group considered to represent a separate cytogenetically defined disease category in the World Health Organization (WHO) classification. Patients with this syndrome, mostly women, are characterized by the presence of isolated deletion 5q, a blast count below 5%, favorable prognosis and a low rate of AML transformation.[2,3] So far, no other characteristic besides the proportion of bone marrow (BM) blasts and the existence of additional chromosomal abnormalities has been recognized and universally accepted as a predictor of outcome for patients with MDS and deletion 5q.[10,11] Further, no variable has been shown to impact the clinical course of patients with WHO-defined '5q−syndrome'. Lenalidomide therapy has activity in single-arm clinical trials in patients with International Prognostic Scoring System (IPSS) low or intermediate-1 risk, red blood cell transfusion dependency and deletion 5q,[12–14] leading to approval by the US Food and Drug Administration for this indication. In contrast, the European Medicines Agency refused approval of lenalidomide for these patients, because there were no historical data against which the safety of lenalidomide could be compared, especially regarding the expected risk of AML transformation.[15] Thus, the analysis of further prognostic parameters for OS and AML transformation in large series of MDS patients with deletion 5q is of importance.

The major aim of this global cooperation study was to assess the characteristics and natural history of a large series of 541 patients with *de novo* MDS and deletion 5q to identify prognostic factors of outcome.

Materials and methods

Patients and diagnostic criteria

A total of 541 patients with primary MDS and deletion 5q, included in the Spanish Haematological Cytogenetic Working

Group/Spanish Registry of MDS (234 patients), German–Austrian MDS Study Group (198 patients), MD Anderson Cancer Center (85 patients), Tokyo Medical University (12 patients) and other centers participating in the International Working Group on MDS Cytogenetics (12 patients) databases were the subject of this analysis. Several patients in this study had been included in previously published reports,[5,9,11] but without focusing on deletion 5q. Cases belonging to the Spanish Haematological Cytogenetic Working Group, Spanish Registry of MDS and MD Anderson Cancer Center were scrutinized and double checked before inclusion for avoiding duplication.

The cases were collected between November 1972 and September 2008. The diagnosis of MDS was made according to the classification proposal of the French–American–British (FAB) study group.[1] Patients with a diagnosis of refractory anemia with excess blasts in transformation or chronic myelomonocytic leukemia by FAB criteria were excluded because they are no longer considered as MDS by the WHO classification system. Whenever possible, patients were reclassified by WHO 2001 criteria.[2] Patients with an ambiguous diagnosis of MDS and those who had previously received chemotherapy or radiotherapy (therapy-related MDS) were excluded. In all patients included in this study, deletion 5q had been detected by conventional cytogenetics. The cytogenetic analysis of BM specimens was performed at the individual centers following standard chromosome-banding procedures, being cross-validated among centers in previously published studies. Inclusion in the study required the analysis of at least 10 metaphases per case. The criteria defined by the International System for Human Cytogenetic Nomenclature in 2005 were used for identification of abnormal clones.[16] For example, a karyotype was considered complex when more than two independent cytogenetic abnormalities were found. When two or more clones with two aberrations were noted, the patient was categorized in the complex aberration group, whereas patients with two karyotypically independent clones with a single change in one clone and two anomalies in the second one were not considered as complex chromosomal abnormalities. Loss of Y chromosome was considered as one chromosomal abnormality. In this series, an unrelated clone was defined as a clone with cytogenetic aberrations that did not derive from the progenitor clone with the deletion 5q. The unrelated clones were considered as additional aberrations, accompanying the deletion 5q, for the definition of its cytogenetic complexity.[17] All the cytogenetic information corresponding to the German–Austrian MDS Study Group was initially reviewed by JS and DH; and the Spanish Haematological Cytogenetic Working Group/Spanish Registry of MDS cytogenetic information by MM, BE and FS. The final revision was carried out by FS, deleting those cases with incomplete cytogenetic information. The final diagnosis was provided by each institution, all of them with recognized experience in this pathology.

In keeping with the guidelines of the Declaration of Helsinki Principles, this retrospective noninterventional study was conducted with the approval of the internal review board from the participating institutions belonging to each registry/cooperative group/center or following individual institutional guidelines.

Prognostic factors

Different patient and disease characteristics, recorded at the time of diagnosis, were examined in the prognostic factor analysis to establish their possible relationship with OS and AML transformation. Basic demographic data included age and sex. Hematological parameters were hemoglobin level, absolute neutrophil count (ANC), platelet count, number of cytopenias and proportion of blast cells in BM, all of them taking cutoff points and groups defined by the 1997 IPSS into account.[10] For platelet count, an additional cutoff point of 150×10^9 per liter was analyzed. Initially, we chose to test this value based on the higher platelet count that characterizes the '5q−syndrome' and the low number of patients with severe thrombocytopenia in this subset. After showing its association with prognosis in those patients, we decided to examine its potential impact in the overall series as well.

Classification systems included FAB[1] and WHO 2001[2] classifications, and IPSS scoring system. The IPSS risk categories considered were those in the original report (low, intermediate-1, intermediate-2 and high).[10] Cytogenetic findings recorded and analyzed were the presence of additional chromosome abnormalities, including the number of additional abnormalities (karyotype complexity) and the most prevalent specific additional abnormalities found (chromosome 1, chromosome 3, −7, 7q−, +8, +11, +13, 12p−, chromosome 17, −18/18q−, 20q−, +21, −X/−Y and unrelated clones, taking into account if they were accompanying deletion 5q as a single additional chromosome abnormality or in the context of a complex karyotype), the proportion of metaphases carrying deletion 5q, and the most frequent break points of the 5q-deleted region (q13q31, q13q33, q22q33, q12q33, q14q34 and other break points). Initially, the number of additional chromosomal abnormalities was grouped into six categories: none (isolated deletion 5q), one, two, three, four and five or more additional abnormalities. After showing that the clinical outcome for patients with two or more additional abnormalities was almost identical, only three cytogenetic categories were considered for all subsequent analysis: isolated deletion 5q, deletion 5q plus one additional abnormality and deletion 5q plus two or more additional abnormalities.

Statistical analysis

Comparisons of proportions and ranks of variables between different groups were performed by χ^2-test, Fisher's exact test, Student's *t*-test, Mann–Whitney *U*-test or one-way ANOVA with *post hoc* Tukey's test, as appropriate.

The Kaplan–Meier product limit method was used to estimate the probability of OS and risk of AML transformation,[18–21] OS was measured from hematological diagnosis to death or last follow-up. All deaths, whether related or not to MDS, were considered as the end point of the follow-up interval. Patients treated with intensive AML-type chemotherapy (11 patients), hematopoietic stem cell transplantation (3 patients) or with lenalidomide (3 patients) were considered as censored data at the time of starting treatment, when the starting date of treatment was available. AML transformation was measured from diagnosis to AML development. Patients dying from any cause before developing AML were considered as censored data in the date of death for the calculation of AML transformation curves. To avoid any potential bias in the estimation of the risk of AML transformation, only patients from those registries/centers with information about AML evolution was available in most of instances were included in the calculation of AML transformation risk. Statistical comparisons between different actuarial curves were based on log-rank tests.[19–21]

Multivariate analysis using the Cox proportional hazards regression method for temporal events was used to identify the most significant independent prognostic variables for OS and AML transformation.[22] Characteristics selected for possible inclusion in the multivariate model were those for which there